https://doi.org/10.5194/acp-2020-809
Preprint. Discussion started: 2 September 2020

Atmospheric Chemistry and Physics Discussions

The effects of morphology, mobility size and SOA material coating on the ice nucleation activity of black carbon in the cirrus regime

Cuiqi Zhang[1,2], Yue Zhang[3,4,5], Martin J. Wolf[2], Leonid Nichman[6], Chuanyang Shen[2,7], Timothy B. Onasch[4,5], Longfei Chen[1], and Daniel J. Cziczo[2,8,9]

[1]School of Energy and Power Engineering, Beihang University, Beijing, China
[2]Department of Earth, Atmospheric, and Planetary Sciences, Massachusetts Institute of Technology, Cambridge, MA 02139, United States
[3]Department of Environmental Sciences and Engineering, University of North Carolina at Chapel Hill, Chapel Hill, NC 27599, United States
[4]Aerodyne Research Incorporated, Billerica, MA 01821, United States
[5]Department of Chemistry, Boston College, Chestnut Hill, MA 02467, United States
[6]National Research Council Canada, Flight Research Laboratory, Ottawa, ON, K1V 9B4, Canada
[7]Department of Atmospheric and Oceanic Sciences, Peking University, Beijing, China
[8]Department of Civil and Environmental Engineering, Massachusetts Institute of Technology, Cambridge, MA 02139, United States
[9]Department of Earth, Atmospheric, and Planetary Sciences, Purdue University, West Lafayette, IN 47907, United States

Correspondence to: Longfei Chen (chenlongfei@buaa.edu.cn)

Abstract. There is evidence that black carbon (BC) particles may affect cirrus formation and hence global climate by acting as potential ice nucleating particles (INPs) in the troposphere. Nevertheless, the ice nucleation (IN) ability of bare BC and BC coated with secondary organic aerosol (SOA) material remains uncertain. We have systematically examined the IN ability of 100-400 nm size-selected BC particles with different morphologies and different SOA coatings representative of anthropogenic (toluene and *n*-dodecane) and biogenic (*β*-caryophyllene) sources in the cirrus regime (-46 to -38 °C). Several aerosolized BC proxies were selected to represent different particle morphologies and oxidation levels. Atmospheric aging was further replicated with exposure of SOA-coated BC to OH. The results demonstrate that the 400 nm hydrophobic BC types nucleate ice only at or near the homogeneous freezing threshold (-42 to -46 ˚C). Deposition IN, as opposed to purely homogeneous freezing, was observed to occur for some BC types between 100-200 nm within the investigated temperature range. More fractal BC particles did not consistently act as superior deposition INPs over more spherical ones. SOA coating generated by oxidizing *β*-caryophyllene with O_3 did not seem to affect BC IN ability. However, SOA coatings generated from OH oxidation of various organic species did exhibit higher IN onset supersaturation ratio with respect to ice (SS_i) compared with bare BC particles, with toluene SOA coating showing an increase of SS_i by 0.1-0.15 while still below the homogeneous threshold. *n*-dodecane and *β*-caryophyllene-derived SOA only froze in the homogeneous regime. We attribute the inhibition of IN ability to the filling of the pores on the BC surface by the SOA material coating. OH exposure levels of all SOA coating experiments, from an equivalent atmospheric 10 days to 90 days, did not render significant differences in IN potential. Our study suggests that BC particles with large sizes and/or oxidized surfaces generally exhibit better IN ability, and that the organic coating materials can inhibit ice formation.

https://doi.org/10.5194/acp-2020-809
Preprint. Discussion started: 2 September 2020

Atmospheric Chemistry and Physics Discussions

1 Introduction

Cirrus clouds affect the global energy balance predominantly by more effectively trapping terrestrial long-wave terrestrial radiation than reflecting solar energy (e.g., Heymsfield et al., 2017; Kärcher, 2018; Kärcher et al., 2007). In cirrus clouds, ice crystals can form via two pathways, i.e. homogeneous and heterogeneous ice nucleation (IN) (Heymsfield et al., 2017; Kanji et al., 2017; Vali et al., 2015). Homogeneous freezing is the spontaneous freezing of solution droplets without any foreign surfaces aiding the process (Heymsfield et al., 2017; Koop et al., 2000; Vali et al., 2015). Heterogeneous IN occurs more readily than homogeneous IN due to the presence of an ice nucleating particle (INP) at a lower supersaturation with respect to ice (SS_i) or warmer temperature (DeMott et al., 2003; Kanji et al., 2017; Vali et al., 2015). Deposition IN is one heterogeneous IN mode, in which solid ice is formed by direct water vapor deposition on to an INP surface.

Aircraft emissions, especially those containing black carbon (BC) aerosols, may be an important direct source of anthropogenic INPs to the tropopause (Burkhardt and Kärcher, 2011; Kärcher, 2018; Petzold et al., 1998; Popovicheva et al., 2004; Seinfeld, 1998). Global mass-based aviation BC emission rates are estimated to range between 2-20 Gg year^{-1} (Bond et al., 2013; Bond et al., 2004; Lee et al., 2010; Zhang et al., 2019a), while the number-based aviation BC emission rate is estimated to be equivalent to ~1.3 % of total ground anthropogenic BC emissions (Zhang et al., 2019a). Aviation fuel usage is projected to increase 2-4 fold in the next few decades (Lee et al., 2009; Lee et al., 2010), simultaneously increasing aircraft-induced cloudiness (Burkhardt and Kärcher, 2011; Kärcher, 2018; Petzold et al., 1998; Popovicheva et al., 2004; Seinfeld, 1998). However, the role of BC aerosol-cloud-climate interactions in cirrus formation remains highly uncertain (IPCC, 2013).

Laboratory experiments have been carried out to simulate the atmospheric environment to study the effects of isolated processes on BC IN ability in detail. Both well-characterized commercially available BC (e.g., Brooks et al., 2014; DeMott et al., 1999; Fornea et al., 2009; Mahrt et al., 2018; Nichman et al., 2019) and soot particles from combustion sources (e.g., Crawford et al., 2011; Diehl and Mitra, 1998; Dymarska et al., 2006; Friedman et al., 2011; Kanji and Abbatt, 2006; Kanji et al., 2011; Koehler et al., 2009; Kulkarni et al., 2016; Möhler et al., 2005b; Mahrt et al., 2018; Nichman et al., 2019) have been used to investigate the IN ability of BC particles, with a particular focus on the deposition IN mode below -38 °C. According to previous studies (e.g., Friedman et al., 2011; Hoose and Möhler, 2012; Koehler et al., 2009; Kulkarni et al., 2016; Mahrt et al., 2018; Nichman et al., 2019), the following physicochemical properties of particles may play vital roles in determining BC deposition IN activity: a) mobility diameter (d_m), b) morphology, c) surface oxidation state, and d) organic material coating. It is widely acknowledged that larger particles act as more efficient INPs (e.g., Pruppacher and Klett, 2010). Although the mechanism remains uncertain, one common theory is that nucleation probability and rate are positively correlated to particle surface area (e.g., Hoose and Möhler, 2012); therefore, larger particles may offer more surface sites for nucleation. The IN ability of monodisperse BC particles with the size range of 100-800 nm has previously been characterized (Friedman et al., 2011; Koehler et al., 2009; Kulkarni et al., 2016; Mahrt et al., 2018; Nichman et al., 2019). The lower size limit at which BC

https://doi.org/10.5194/acp-2020-809
Preprint. Discussion started: 2 September 2020


Atmospheric Chemistry and Physics Discussions

particles act as active deposition INPs below -38 °C varied between 100 nm and 400 nm. However, the size threshold below which BC cannot nucleate ice in deposition mode and the underlying mechanism is still uncertain.

Laboratory experiments and field observations confirmed that BC morphology and surface chemistry may change significantly during the atmospheric aging processes, leading to changes in particle surface area, shape, and chemical composition (e.g., China et al., 2015; Fu et al., 2012; Li et al., 2017; Li et al., 2016; Moffet et al., 2016; Slowik et al., 2007; Tritscher et al., 2011; Wang et al., 2017). Commonly-used BC morphology characteristics are those derived from 2-D projected electron microscopy images, including fractal dimension (D_f), roundness, aspect ratio (AR), and convexity (e.g., China et al., 2013; China et al., 2014; China et al., 2015; Kulkarni et al., 2016; Lee and Kramer, 2004; Ramachandran and Reist, 1995). Effective density and surface area have also been utilized to reflect BC morphology and mixing state (Kulkarni et al., 2016; Mahrt et al., 2018; Nichman et al., 2019; Tritscher et al., 2011).

Freshly emitted BC particles are typically hydrophobic, fractal, nanoscale (<200 nm) aggregates with a branched or chain-like structure (e.g., Beyersdorf et al., 2014; Kinsey et al., 2010; Liati et al., 2014; Lobo et al., 2015; Moore et al., 2017; Vander Wal et al., 2014). BC aggregate surface area is determined by primary particle sizes, number of primary particles, and the way primary particles are connected (Kittelson, 1998; Kumfer and Kennedy, 2009). Mahrt et al. (2018) and Nichman et al. (2019) reported a positive correlation between BC particle surface area and IN activity for particles with same size. They attributed BC IN activity to pore condensation and freezing (PCF) mechanism (David et al., 2019; Koop, 2017; Marcolli, 2014, 2017), in which deposition freezing of BC was considered essentially homogeneous freezing of liquid water taken up in mesopores (2-50 nm) due to capillary effect (Berg, 2009; Bikerman, 1978; Liu and Cao, 2016).

The surface chemistry of the emitted particles is governed by the source and the host environment in which the particles evolve. Nascent BC particles can interact with volatile species such as sulfates and unburnt hydrocarbons in the aircraft cooling exhaust plume and grow (e.g., Anderson et al., 2011; Kärcher, 2018; Lefebvre, 1998; Onasch et al., 2009). These particles can remain suspended in the atmosphere for days to weeks, during which the exposure to atmospheric biogenic and anthropogenic species, as well as oxidation, can lead to complex secondary organic aerosol (SOA) coatings (Kulkarni et al., 2016). Numerous experiments have been conducted to investigate the effects of surface coating on BC deposition IN ability. Hygroscopic BC particles (Koehler et al., 2009), or BC particles coated by hygroscopic materials, such as sulfuric acid (Crawford et al., 2011; DeMott et al., 1999; Möhler et al., 2005b), water-soluble organic acids (Friedman et al., 2011; Nichman et al., 2019) and SOA (Kulkarni et al., 2016), tended to enhance BC water uptake ability and form aqueous solutions on BC surface, moving IN onset SS_i towards the homogeneous freezing threshold. Hydrophobic organic coatings tended to impede surface interaction between BC and water molecules. Möhler et al. (2005b), Crawford et al. (2011), and Mahrt et al. (2018) reported a transition from heterogeneous to homogeneous freezing mode for combustion BC with increasing OC content. Ozone (Friedman et al., 2011) and hydroxyl (OH) radical (Chou et al., 2013; Kulkarni et al., 2016) oxidation can change surface functional groups of BC particles and enhance hydrophilicity, but no distinguishable BC IN activity change has been observed. Despite these previous

https://doi.org/10.5194/acp-2020-809
Preprint. Discussion started: 2 September 2020


Atmospheric Chemistry and Physics Discussions

efforts, the influence of particle morphology, chemistry, and aging, as well as the microphysical mechanism behind BC deposition IN ability, remains ambiguous.

In this work, we examine the effects of particle mobility diameter, morphology, and SOA coating on the IN ability of several aerosolized BC proxies as a function of SS_i in a cirrus relevant temperature regime (from -46 °C to 38 °C). Representative species of anthropogenic (toluene and *n*-dodecane) and biogenic (β-caryophyllene) volatile organic compounds were chosen to simulate potential photochemical atmospheric aging processes of BC. Different aging durations in equivalent atmospheric times were simulated by controlling the OH radical exposure. Our results help to clarify the effects of physicochemical properties and SOA formation on BC IN ability and cirrus formation in the upper troposphere.

2 Experimental: materials and methods

2.1 Materials

2.1.1 Black carbon samples

Three types of commercially available BC particles (Raven 2500 Ultra, hereafter R2500U, Birla Carbon U.S.A., Inc.; REGAL 330R, hereafter R330R, Cabot Corporation; and CAB-O-JET 300, hereafter COJ300, Cabot Corporation Inkjet Colorants Division), corresponding to different surface chemistry and morphology regimes were studied as proxies of atmospheric BC. Table 1 summarizes the characteristics of these BC proxies. R2500U and R330R are carbonaceous black pigment powder generated by incomplete combustion. COJ300 is a highly dispersible ink due to the 4-carboxyphenyl-modified surface (Johnson, 1999). COJ300 is selected for its high degree of oxidation, which is confirmed by the Particle Analysis by Laser Mass Spectrometry (PALMS) chemical analysis (see Fig. A1), classifying it as the most oxidized BC proxy in this study. R2500U and R330R are unoxidized but differ in morphology, which was confirmed by morphology characterization and PALMS analysis (see Sect. 3.1). R2500U, R330R, and COJ300 were chosen as proxies of freshly emitted BC, atmospheric compacted BC, and atmospheric oxidized BC, respectively. IN properties of 800 nm R330R and R2500U particles were previously studied (Nichman et al., 2019). This work addresses the remaining questions raised in the previous study and focuses on the impact of particle size, morphology, and surface oxidation.

2.1.2 SOA coating materials

Three organic species, toluene, *n*-dodecane, and β-caryophyllene, were selected to represent atmospheric SOA precursors from anthropogenic and biogenic sources (Table S1). Toluene and *n*-dodecane are often selected as surrogate jet fuel components to investigate combustion and emission characteristics because they have been proven well-suited to represent tens of hundreds of components found in mainstream jet fuels (e.g., Dooley et al., 2010; Dooley et al., 2012; Zhang et al., 2016; Zhao et al., 2017). Field aircraft emission studies also confirm the presence of these unburnt aliphatic and aromatic organic compounds in aircraft engine exhaust (e.g., Beyersdorf et al., 2012; Kinsey et al., 2011; Pison and Menut, 2004; Timko

https://doi.org/10.5194/acp-2020-809
Preprint. Discussion started: 2 September 2020

Atmospheric Chemistry and Physics Discussions

et al., 2014). These organic compounds may coat BC particles, forming BC-containing aerosols in engine plume. Moreover, toluene is considered a dominant aromatic SOA precursor due to anthropogenic activities (e.g., Pandis et al., 1992) and serves as a proxy for other light aromatic species in atmospheric aromatic-seeded SOA formation models (e.g., Hildebrandt Ruiz et al., 2015). *n*-dodecane is one of the most studied long-chain aliphatic SOA precursor (e.g., Loza et al., 2014; Presto et al., 2010; Yee et al., 2013) representing less volatile aliphatic species. *β*-caryophyllene has been found to be one of the most atmospherically abundant sesquiterpenes (Ciccioli et al., 1999; Guenther et al., 2012; Henrot et al., 2017). Due to its high reactivity towards ozone and hydroxyl radical to form oxidized products with low volatility, *β*-caryophyllene has a strong potential to form biogenic SOA in the atmosphere (Calogirou et al., 1997; Griffin et al., 1999; Hoffmann et al., 1997; Lee et al., 2006).

2.2 BC particle generation and characterization

2.2.1 BC particle generation

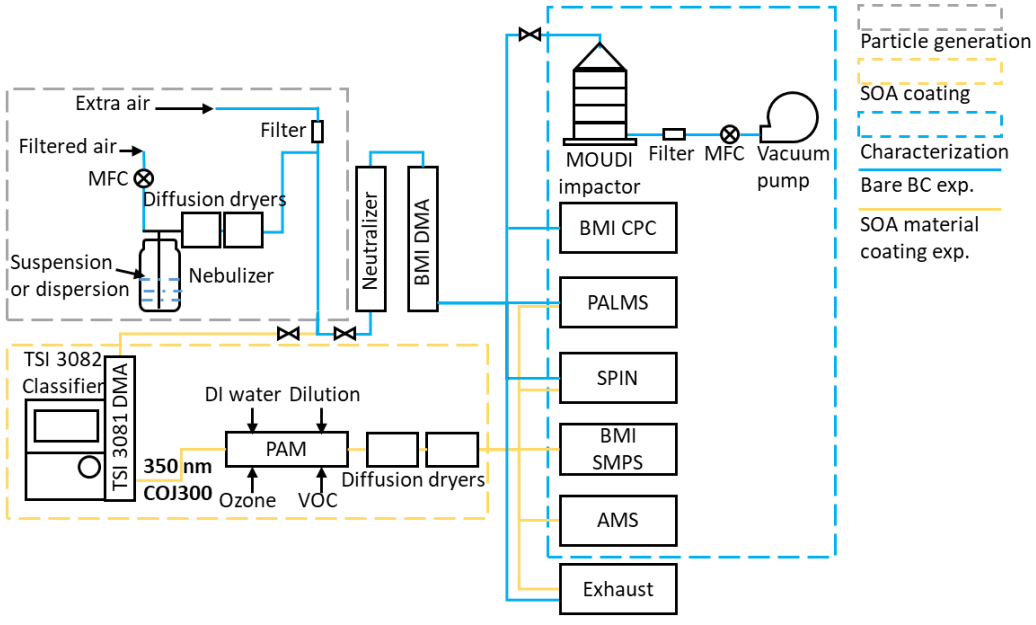

Figure 1. Schematic diagram of the experimental apparatus for bare BC particles (blue lines) and organic SOA coating experiments (yellow lines). The grey dashed box encloses the particle generation section, which is used for both bare BC and organic SOA coating experiments. The yellow dashed box denotes the SOA coating section. The blue dashed box is the aerosol characterization and test section.

Figure 1 shows a schematic diagram of the experiment apparatus used in this study. The particle generation setup is enclosed in the grey dashed box. Suspensions of R2500U and R330R, as well as a diluted COJ300 dispersion (dilution ratio 1:30) were atomized with a 3-jet collision nebulizer (CH Technologies (USA), Inc.), and bare BC experiments are marked by blue lines in Fig. 1. Suspensions of BC powder (R2500U and R330R) were prepared by mixing 1 g BC powder with 100 mL

https://doi.org/10.5194/acp-2020-809
Preprint. Discussion started: 2 September 2020


Atmospheric Chemistry and Physics Discussions

de-ionized (DI) water. The mixture was then sonicated for 10 minutes to make the suspension more uniform. The flow rate through the nebulizer was 1.5 SLPM (standard liters per minute), controlled by a mass flow controller (MFC, Model MC-2SLPM-D; ALICAT Scientific). The atomized BC particles were dried by passing them through two consecutive 43 cm silica gel diffusion dryers (DDU 570/H, Topas). All samples were then neutralized and size selected by a BMI differential mobility analyzer (BMI DMA, Model 2002; Brechtel Manufacturing Inc.) or TSI DMA (Model 3081, Classifier, Model 3082; TSI Inc.) for bare BC and BC-SOA mixing experiments, respectively. The relative humidity (*RH*) of the aerosol stream entering the DMA measured by the BMI built-in *RH* sensor was ~16 %. During the BC ice nucleation experiments, the size-resolved particle number concentration was monitored with a BMI condensation particle counter (BMI CPC, Model 1700; Brechtel Manufacturing Inc.).

2.2.2 Characterization of BC morphology

The 200 nm, 300 nm and 400 nm R2500U, and 400 nm R330R and COJ300 BC particles were collected on 300-mesh carbon film copper grids (Ted Pella, Inc.) with a MOUDI impactor (Model M135-10; TSI Inc.) for offline morphology analysis. The flow rate through the impactor was controlled by a MFC (Model MC-5SLPM-D; ALICAT Scientific) at 2 SLPM so that the cut-off size of the impactor was 100 nm. The samples were analyzed offline in a Zeiss Merlin High-resolution Scanning Electron Microscopy (HRSEM; Carl Zeiss Microscopy GmbH).

Table 1. Characteristics of selected BC proxies in this study. $\boldsymbol{a_{BET-N_2}}$ is the BET specific surface area based on N_2 adsorption isotherms; $\boldsymbol{d_m}$ is the particle mobility diameter; $\overline{\boldsymbol{d_a}}$ denotes the mean 2-D projected area-equivalent aggregate diameter derived from SEM images; mean aspect ratio ($\overline{\boldsymbol{AR}}$), roundness ($\overline{\boldsymbol{Roundness}}$) and circularity ($\overline{\boldsymbol{Circularity}}$) are the geometric mean morphology parameters derived from several aggregates and are defined in Sect. 2.2.2; $\overline{\boldsymbol{d_{pp}}}$ denotes the mean geometric diameter of primary particles measured from SEM images, and $\boldsymbol{N}$ the number of primary particles analyzed for each BC type and size; $\boldsymbol{D_f}$ denotes the 3-D fractal dimension derived from 2-D SEM images; $\boldsymbol{d_{va}}$ is the particle vacuum aerodynamic diameter measured by the Particle Analysis by Laser Mass Spectrometry (PALMS) instrument; values in parenthesis are the corresponding standard deviation.

BC type	**R2500U**	**COJ300**	**R330R**
Composition	Furnace black	(4-carboxyphenyl)-modified carbon black[a]	Furnace black
CAS No.	1333-86-4	1106787-35-2	1333-86-4
Specific gravity (20 °C)	1.7-1.9[a]	1.07 (dispersion)[a]	1.7-1.9[a]
Bulk density (g/cm^3)	20-380	-	20-380

https://doi.org/10.5194/acp-2020-809
Preprint. Discussion started: 2 September 2020

Atmospheric Chemistry and Physics Discussions

pH		7.0[b]; 4-11[c]		7.0-8.6[a]	6.9[b]; 2-11[c]
Solubility		Insoluble		Insoluble but dispersible	Insoluble
a_{BET-N_2} **(m²/g)**[a,d]		270		200	90
d_m **(nm)**	200	300	400	400	400
$\overline{d_a}$ **(nm)**	316.9	403.5	343.5	629.4	816.6
	(109.3)	(82.5)	(106.3)	(308.3)	(355.3)
$\overline{AR}$	1.22	1.36	1.44	1.19	1.33
	(0.16)	(0.27)	(0.29)	(0.17)	(0.28)
$\overline{Roundness}$	0.81	0.77	0.73	0.84	0.75
	(0.06)	(0.08)	(0.09)	(0.08)	(0.10)
$\overline{Circularity}$	0.78	0.64	0.61	0.72	0.53
	(0.18)	(0.14)	(0.15)	(0.20)	(0.16)
$\overline{d_{pp}}$ **(nm)**	41.9	35.5	34.5	34.2	45.4
	(12.4)	(9.9)	(11.4)	(9.9)	(13.6)
N	242	256	343	139	251
D_f	2.02	1.92	1.92	2.34	2.31
Median d_{va}[e]	-	-	608.7	610.6	-
Effective density (g/cm³)[f]	-	-	1.52	1.44	-
Median O:C ratio[g]	-	-	0	0.02	-

[a]Information offered by manufacturer datasheet. [b]Measured by Nichman et al. (2019) using VWR pH meter. [c]Measured by manufacturer in compliant with ASTM 1512. [d]BET specific surface area measured by manufacturers using N_2 adsorption in compliant with ASTM D-4820. [e]Converted from the measured time of flight. [f]Calculated from dividing median d_{va} by d_m (400 nm in this study) and times the reference density 1 g/m³ (Cziczo et al., 2006). [g]Calculated from PALMS spectra area.

Table 1 summarizes the morphological characteristics, including the projected area-equivalent diameter (d_a), aspect ratio (AR), roundness, circularity, and 3-D fractal dimension (D_f), for different BC types and sizes derived from high resolution SEM images (×30,000 to ×150,000). Primary particle diameter ($\overline{d_{pp}}$) is the geometric average of the length and width of a

https://doi.org/10.5194/acp-2020-809
Preprint. Discussion started: 2 September 2020


Atmospheric Chemistry and Physics Discussions

clear primary particle (Fig. A2 and A3). $d_a = \sqrt{4A_a/\pi}$ is the diameter of a spherical aggregate that has the same projected area (A_a) as the BC aggregate (China et al., 2014). $AR = L_{max}/W_{max}$ is the ratio between the longest dimension (L_{max}) of an aggregate periphery to the perpendicular maximum width (W_{max}, Fig. A2). $Roundness = \sqrt{4A_a/\pi L_{max}{}^2}$ is used as a BC aggregate shape descriptor (e.g., China et al., 2013; China et al., 2015; Kulkarni et al., 2016). Both *AR* and roundness are used to represent shape deviation from a circle, whose *AR* and roundness equal 1. $Circularity = 4\pi A_a/p^2$ is a parameter used to describe the rugged level of an aggregate periphery, with rugged irregular periphery causing circularity smaller than 1. D_f depends on primary particle number (N) and radius of gyration (R_g) of the aggregate (Mandelbrot, 1982). By using an ensemble approach, N is found to be scaled with $(A_a/A_p)^{1.09}$, where A_a and A_p are projected area of aggregate and primary particles, respectively (China et al., 2014; Köylü et al., 1995; Oh and Sorensen, 1997; Samson et al., 1987). The approximate relation $L_{max}/2R_g = 1.50 \pm 0.05$ iss used to substitute R_g, (Brasil et al., 1999), and yield $k\,(L_{max}/\overline{d_p})^{D_f} = (A_a/A_p)^{1.09}$. D_f can then be derived by a power law fit of scattered points between $L_{max}/\overline{d_p}$ and $(A_a/A_p)^{1.09}$ for each aggregate (Fig. A4).

2.2.3 Chemical composition characterization of single BC particle

Qualitative chemical composition of monodisperse BC particles was determined by PALMS. The detailed description of PALMS can be found elsewhere in literature (Cziczo et al., 2006; Zawadowicz et al., 2015). PALMS is an online single particle mass spectrometer in which inlet particles are first aligned by an aerodynamic lens. Two Nd:YAG green (532 nm) laser beams separated by 33.6 mm are arranged at the bottom of the inlet, measuring particle velocity based on time gap between the scattering signals. The velocity can be converted into vacuum aerodynamic diameter (d_{va}) from the measured time of flight (Cziczo et al., 2006, Fig. A5). A 193 nm ultraviolet (UV) excimer laser is then triggered, ablating and ionizing the particle. The ions of both refractory and volatile particle components are classified based on their mass to charge (m/z) ratio. PALMS provides either positive or negative polarity spectra for each particle. Particle ionization is often not quantitative. However, average ion ratios across many spectra allows a qualitative compositional comparison between two similar aerosol populations. Hundreds of spectra were collected for each soot sample to account for ionization difference caused by particle orientation difference (Murphy et al., 1998).

Chemical composition of the SOA-coated BC particle stream was analyzed online by PALMS and an Aerosol Mass Spectrometry (AMS; Aerodyne Research Inc.). The AMS offers quantitative average mass spectrum of an ensemble of aerosols. Particles entering AMS first go through an aerodynamic lens inlet to form a particle beam. A mechanical chopper is used downstream the inlet to control sampling particle or particle free period. The AMS employs a heated 600 °C tungsten surface to vaporize nonrefractory aerosols. Ionization is achieved using a universal 70 eV electron ionization technique. Ionized species are detected by time of flight mass spectrometry. More details about AMS can be found in literatures (Jayne et al., 2000; Onasch et al., 2012).

https://doi.org/10.5194/acp-2020-809
Preprint. Discussion started: 2 September 2020


Atmospheric Chemistry and Physics Discussions

2.3 SOA material coating on BC particles

The 350 nm COJ300 BC was chosen to be the seed particle in all SOA coating experiments because of its effective IN activity as well as its higher particle concentration (~1×10^6 # L^{-1}) at the selected size in comparison with other BCs (1-3 × 10^4 # L^{-1}).

Particle generation during the SOA coating experiments was identical to bare BC experiments. The SOA coating experimental setup section is enclosed in the yellow dashed box of Fig. 1. COJ300 BC particles were nebulized in an air flow of 2.2 SLPM and dried in two consecutive 43 cm silica gel diffusion dryers, and then 350 nm BC particles were size-selected by a TSI 3081 DMA, and directed to a potential aerosol mass (PAM) oxidation flow chamber (Kang et al., 2007; Lambe et al., 2011a; Liu et al., 2018). In the PAM reactor, gas phase volatile organic compound (VOC) reacts with OH radical and/or O_3 (Lambe et al., 2011a; Zhang et al., 2018a), and subsequently form SOA-coated BC particles. All flow rates were controlled by MFCs. The PAM chamber was operated at 4.4 SLPM total flow rate, including 2.2 SLPM BC aerosol flow, 1.0 SLPM O_3 carrier flow, 0.7 SLPM VOC carrier flow and 0.5 SLPM humidified air. The residence time of particles in PAM under such flow condition was approximately 260 s. O_3 was generated by irradiating 1.0 SLPM dry air through an external mercury lamp (λ= 185 nm, AnaLamp low pressure Hg lamp; BHK Inc.) with a concentration of 110 ppm inside the PAM chamber in our study (Lambe et al., 2011b). 0.5 SLPM humidified air was introduced into the chamber to react with the oxygen radical and produce OH radicals, with four mercury lamps (λ = 254 nm; BHK Inc.) mounted in Teflon-coated quartz cylinders inside the chamber to irradiate O_3 and produce oxygen radical ($O(^1D)$) via the UV pyrolysis reaction of O_3 first: $O_3 + h\nu \rightarrow O_2 + O(^1D)$, $O(^1D) + H_2O \rightarrow 2OH$. The OH radical concentration can be varied by changing the four lamps' voltage. Two voltage levels, i.e. 10 V and 3V, were tested in this study (indicated in Table 2 as suffixes *-10* and *-3*), corresponding to different OH exposure levels and atmospheric aging time, ~10-15 days and ~70-90 days based on previous calculation (Lambe et al., 2011a). The VOC was injected into a heated bulb by a syringe pump and mixed with 0.7 SLPM dry air. The particle size distributions downstream of the PAM were measured by a BMI scanning mobility particle sizer (BMI SMPS, comprising a Model 2002 DMA and a Model 1700 CPC; Brechtel Manufacturing Inc.). The injection rate was controlled so that the mode diameter of the particles shifted from 350 nm bare BC particles to 400 nm SOA-coated BC particles, as illustrated in Fig. 2. The 400 nm SOA-coated BC particles were then dried to ~16% *RH* and kept below 25% by passing through two consecutive 43 cm silica gel diffusion dryers (DDU 570/H, Topas). The PAM chamber was cleaned by flushing 10 SLPM clean air overnight after each experiment. In order to confirm the cleanliness of the chamber, particle concentration was measured before and after each experiment.

https://doi.org/10.5194/acp-2020-809
Preprint. Discussion started: 2 September 2020

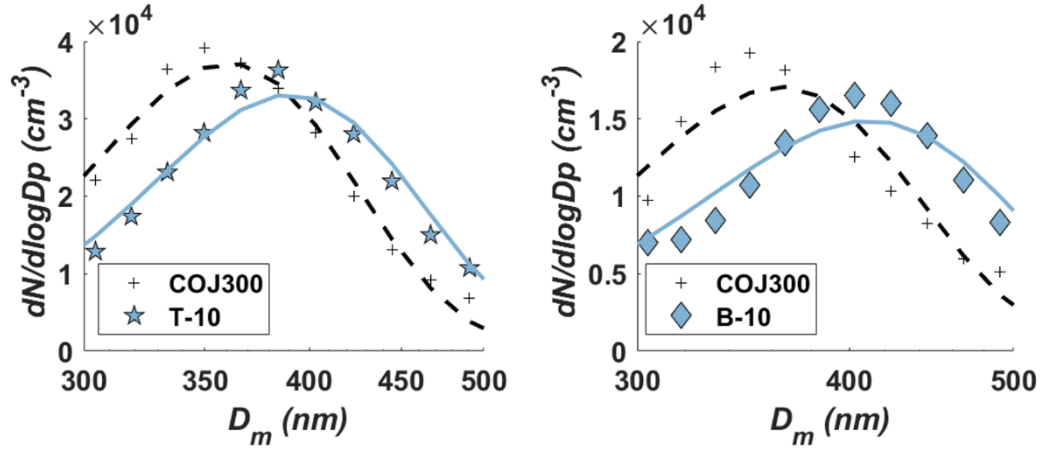

Figure 2. The mode diameter shift of 350 nm COJ300 BC particles after toluene (left panel) and *β*-caryophyllene (right panel) SOA coating. The dashed and solid lines are fitted curves to bare uncoated and coated particles, respectively.

Table 2 summarizes all the SOA mixing IN experiments and the operating conditions. A peak shift from 350 nm to 400 nm and an increase of the 400 nm particle concentrations was observed for all experiments (Fig. 2 and Fig. B1), implying SOA coating on BC particles. The name prefixes *BG*, *T*, *D*, *B* in Table 2 stand for background test, toluene SOA coating experiments, *n*-dodecane SOA coating experiments, and *β*-caryophyllene SOA coating experiments, respectively. The name suffixes *BC*, *0*, *3*, *10*, and *s* denote seed BC only, O_3 oxidation only, low OH exposure level (3 V), high OH exposure level (10 V) and SOA self-nucleation experiments, respectively. All three organic species were exposed to both low and high OH concentrations to investigate the effect of oxidation level on SOA formation and IN activity. An extra O_3 oxidation experiment (*B-0*) was performed for *β*-caryophyllene because it is highly reactive towards O_3 and may form SOA absent of OH. Self-nucleation IN experiments (-*s*) were performed for pure SOAs generated from each organic species to exclude the effect of nucleated pure SOAs mixing with SOA-coated BC particles.

Table 2. Experiment conditions of BC and SOA coating experiments. The name prefixes *BG*, *T*, *D*, *B* stand for background test, toluene SOA coating experiments, *n*-dodecane SOA coating experiments, and *β*-caryophyllene SOA coating experiments, respectively. The name suffixes *BC*, *0*, *3*, *10*, and *s* denote seed BC only, O_3 oxidation only, low OH exposure level, high OH exposure level and SOA self-nucleation experiments, respectively.

Exp. Name	O_3 (ppm)	OH UV Lamp Voltage (V)	Equivalent Atmospheric Exposure (days)	BC Seed	VOC concentration (ppb)[a]	
BG-BC	0	0	0	Y	-	-
BG-0	110	0	0	Y	-	-
BG-10	110	10	70-90	Y	-	-

https://doi.org/10.5194/acp-2020-809
Preprint. Discussion started: 2 September 2020

T-10	110	10	70-90	Y	toluene	6000
T-3	110	3	10-15	Y	toluene	2000
T-s[b]	110	10	70-90	N	toluene	4000
D-10	110	10	70-90	Y	*n*-dodecane	2000
D-3	110	3	10-15	Y	*n*-dodecane	500
D-s[b]	110	10	70-90	N	*n*-dodecane	2000
B-10	110	10	70-90	Y	*β*-caryophyllene	5000
B-3	110	3	10-15	Y	*β*-caryophyllene	2300
B-0	110	0	0	Y	*β*-caryophyllene	5000
B-s[b]	110	10	70-90	N	*β*-caryophyllene	5000

[a]Estimated base on VOC volume injection rate. [b]SOA self-nucleation experiments kept the same OH exposure level and SOA size distribution as corresponding SOA coating experiments

2.4 Ice nucleation measurement

BC IN properties, including conditions at ice nucleation onset and activation fraction (*AF*) as a function of SS_i and temperature, were measured with the SPectrometer for Ice Nuclei (SPIN, Droplet Measurement Technologies). The structure, dimension and operating principles of SPIN can be found in previous studies (Garimella et al., 2016; Nichman et al., 2019; Wolf et al., 2019), and a brief description is given here.

SPIN is a continuous flow diffusion chamber style instrument comprising two flat parallel stainless-steel walls whose temperatures are controlled independently. The sampling flow rate of SPIN is 1.0 SLPM. Particles fed into SPIN are constrained by a ~9.0 SLPM sheath gas within a lamina near the centerline. Turbulent mixing at the injection point causes some particles to spread outside of the aerosol lamina centerline. Since particles experience lower *RH* as they spread outside of the lamina, correction factors ranging from ~1.9 to 8.0 were considered in previous studies (Garimella et al., 2017; Nichman et al., 2019; Wolf et al., 2019). Both walls are coated with ~1 mm ice prior to experiments. At the beginning of each experiment, a linear temperature gradient and water vapor partial pressure field are established between the warm and cold walls. Supersaturation with respect to ice is achieved because of the exponential relationship between temperature and saturation vapor pressure. For all the experiments in this study, SPIN was operated in a SS_i scanning mode (1.0 to 1.6) while keeping the lamina temperature (-46 to -38 °C) constant for each scan. The SS_i increased from 1.0 at a rate of 0.03 per minute by increasing temperature gradient between the walls above homogeneous IN threshold and then lowered to ice saturation.

https://doi.org/10.5194/acp-2020-809
Preprint. Discussion started: 2 September 2020


Atmospheric Chemistry and Physics Discussions

An optical particle counter (OPC) collects scattering signals for number counting and sizing, and a forward scattering depolarized signal for phase discrimination at SPIN chamber outlet. The size detection range of the OPC is 0.5 to 15 μm. A machine learning algorithm using the OPC scattering and laser depolarization signal (Garimella et al., 2016) was used to classify each particle as an inactivated aerosol or ice crystal over the course of an experiment.

We define the IN onset as 1% of particles activating, i.e. *AF* = 1%, for a period of 10 s as activation correction factor of 3.4 and 2.2 was applied for R2500U and R330R (Wolf et al., 2019). Here the *AF* is defined as the number concentration of ice crystals identified by the machine learning algorithm divided by the total particle number concentration entering SPIN. For the size-selected bare BC experiments, the total particle number concentration was measured by a CPC operating simultaneously with SPIN, while for the SOA coating experiments, the total particle number concentration was integrated from the SMPS measurement.

3 Results and discussion

3.1 Ice nucleation on bare BC particles

Figure 3 summarizes (A) deposition IN onset temperature versus SS_i for 100-400 nm (a) R2500U, (b) COJ300 and (c) R330R BC particles; (B) SEM images of bare monodisperse ~400 nm BC particles; (C) representative negative-ion PALMS mass spectra of bare monodisperse ~400 nm BC particles, respectively. Representative error bars in black lines show one standard deviation of variability for SPIN lamina temperature and SS_i, respectively (Kulkarni and Kok, 2012).

As shown in Table 1 and Fig. 3, the three test BC types are substantially different in particle morphology. 400 nm R2500U has the smallest D_f (~1.9), and COJ300 and R330R have larger D_f (~2.3); R2500U is the most fractal BC while COJ300 and R330R are more spherical and compact. Meanwhile, R2500U and COJ300 have similar $\overline{d_{pp}}$ (34-35 nm), and R330R has larger (~45 nm) primary particles. The larger $\overline{d_{pp}}$ of 200 nm R2500U might result from the fusion of primary particles under high magnification. Single particle surface area can be inferred by combining fractal level and $\overline{d_{pp}}$ together, and the decreasing order of single particle surface area is R2500U > COJ300 > R330R, which is in agreement with BET specific surface area data. Negative polarity mass spectra collected for 400 nm BC particles with PALMS are presented in Fig. 3C. The spectra of all three BC types exhibit typical consecutive carbon peaks (*m/z* = 12, 24, 36, etc.). The spectra of COJ300 shows presence of oxidized ions, such as O^- (*m/z* = 16), OH^- (*m/z* = 17), and $COOH^-$ (*m/z* = 45), which are highlighted in red in Fig. 3C(b). The PALMS O:C ratio result confirms that COJ300 is more oxidized than R2500U (Fig. A1).

https://doi.org/10.5194/acp-2020-809
Preprint. Discussion started: 2 September 2020

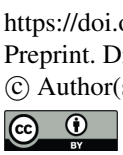

Atmospheric Chemistry and Physics Discussions

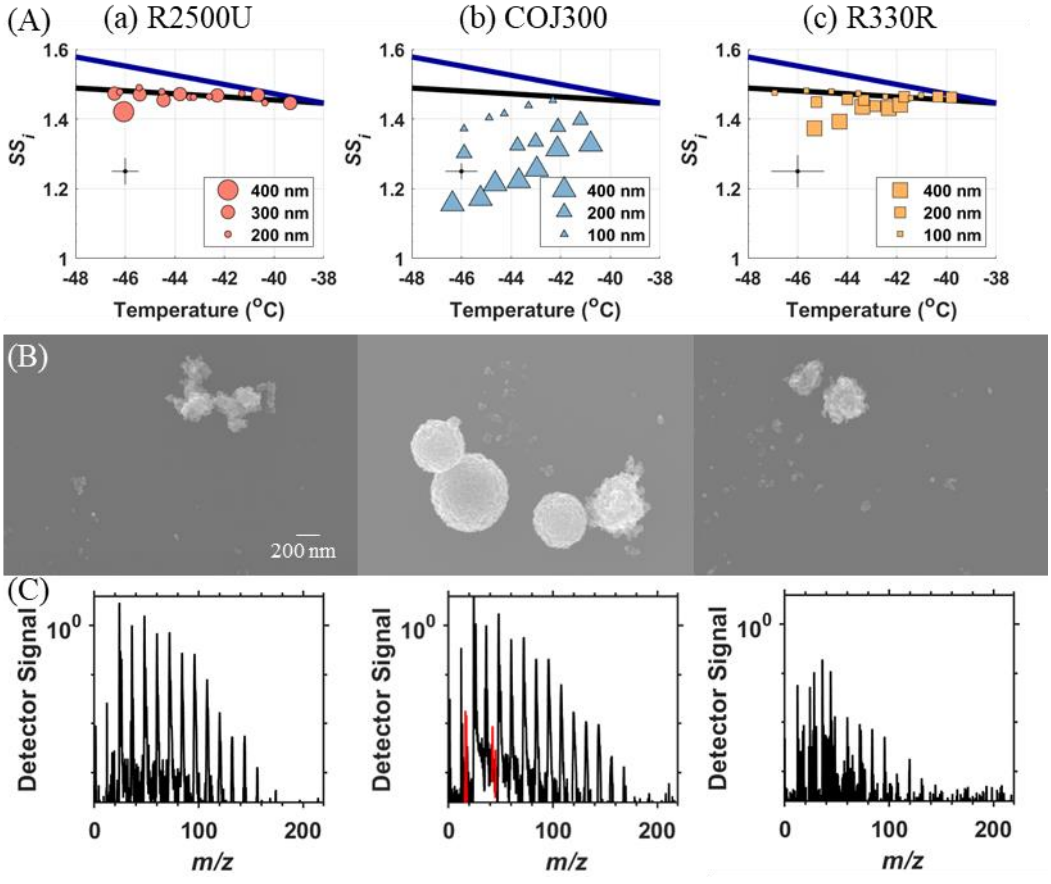

Figure 3. (A) IN onset SS_i (AF = 1%) phase diagram, (B) SEM images, (C) representative negative mass spectrum obtained from PALMS of bare (a) R2500U (pink circles ●), (b) COJ300 (blue triangles ▲), and (c) Regal 330R (yellow squares ■), respectively. Different marker sizes in row (1) corresponds to different d_m. Solid blue lines in row 1 are the water saturation lines, and black lines are homogeneous freezing lines of 200 nm aqueous droplets (Koop et al., 2000). A representative temperature and SS_i error bar is given on the left for each panel. SEM images and PALMS spectrum are for 400 nm BC particles.

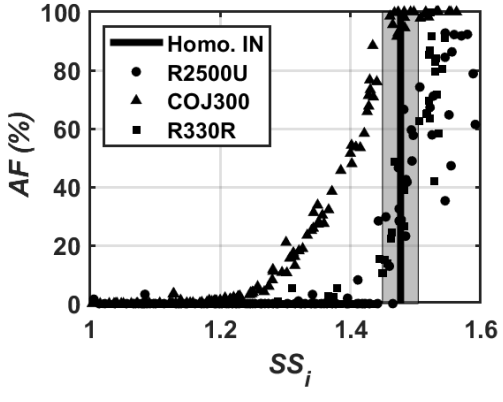

https://doi.org/10.5194/acp-2020-809
Preprint. Discussion started: 2 September 2020


Atmospheric Chemistry and Physics Discussions

Figure 4. -45 °C SS_i scan of 400 nm bare BC particles, showing *AF* as a function of SS_i. The black line is the homogeneous freezing threshold for 200 nm aqueous droplets at -45 °C (Koop et al., 2000). The grey shading indicates one standard deviation of variability for SPIN lamina SS_i.

The results in Fig. 3A demonstrate that the particle size is relevant to particle IN ability. The 400 nm R2500U and R330R BC particles were able to nucleate ice below the homogeneous freezing threshold within the representative uncertainty in the temperature range of -46 to -38 °C. The COJ300 BC particles exhibited deposition IN activity regardless of particle size and temperature in this study. The IN onset SS_i of all depositional active BC particles increases with increasing temperature. The trend is in agreement with previous studies on in cirrus temperature regime (Chou et al., 2013; DeMott et al., 1999; Koehler et al., 2009; Kulkarni et al., 2016; Möhler et al., 2005a; Mahrt et al., 2018; Nichman et al., 2019). The IN onset SS_i of 200 and 300 nm R2500U, as well as 100 and 200 nm R330R, falls into the homogeneous freezing regime. The sharp *AF* increase of 400 nm R2500U and R330R in Fig. 4 confirm that these two BC types nucleate ice via homogeneous freezing. We conclude that the lower size threshold where the IN mode transitions from heterogeneous IN to homogeneous freezing may well lie between 300-400 nm and 200-400 nm for R2500U and R330R around -46 °C, respectively. The IN ability of different size R330R particles at warmer temperature (above -45 °C) shows little difference, indicating that the lower size threshold for R330R is likely between 400-800 nm for temperature between -44 to -40 °C (Nichman et al., 2019). The COJ300 BC is more IN active compared with R2500U and R330R. The COJ300 particles show deposition IN ability below homogeneous freezing threshold down to 100 nm within the temperature range in this study; the lower size threshold for COJ300 is below 100 nm. This finding agrees with the lower size limit between 100 nm and 200 nm for BC particles to act as an active INP reported by Mahrt et al. (2018).

The IN onset results show no clear dependence on particle fractal level and surface area. Even though the more fractal and branching feature of R2500U BC particles may imply that there are more potential surface defects to initiate IN, the R2500U particles do not clearly exhibit superior IN activity over R330R. Koehler et al. (2009) showed that IN was favored for oxidized hydrophilic BC, but too many hydrophilic active sites may bond water molecules, impeding ice embryo formation and thus impair IN (Pruppacher and Klett, 2010). The surface modified, highly dispersible and spherical COJ300 with smaller $\overline{d_{pp}}$ shows better IN efficiency than fractal BC, which is consistent with the results of Mahrt et al. (2018) and Nichman et al. (2019) based on PCF mechanism. The smaller $\overline{d_{pp}}$ offers smaller cavities on particle surfaces that can accommodate liquid water below bulk water saturation by the inverse Kelvin effect (David et al., 2019; Koop, 2017; Marcolli, 2014, 2020). Water saturation pressure drop as a function of cavity radius is shown in Fig. C1 (Marcolli, 2020).

3.2 Ice nucleation on BC coated with SOA material

Figure 5 shows the IN onset SS_i at which 1% of 400 nm SOA-coated COJ300 particles nucleate ice within the temperature range of -46 to -38 °C. The IN onset data of the bare 350 nm COJ300 particles (marked as + symbol) are also included to

https://doi.org/10.5194/acp-2020-809
Preprint. Discussion started: 2 September 2020

Atmospheric Chemistry and Physics Discussions

highlight the effect of SOA coating. IN onset SS_i of pure SOA particles are shown as an asterisk separately to rule out the possible deposition IN induced by pure SOA.

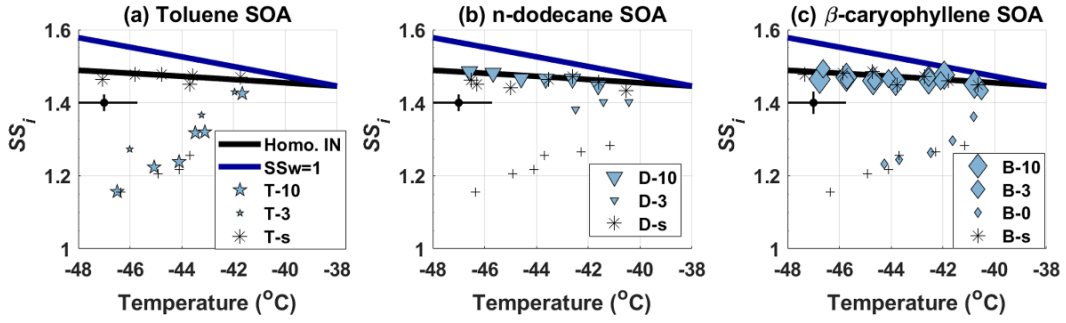

Figure 5. IN onset SS_i phase diagram of 350 nm COJ300 BC particles coated with (a) toluene SOA; (b) *n*-dodecane SOA; (c) *β*-caryophyllene SOA. Different symbol sizes denote different OH exposure level. IN onset SS_i of 350 nm bare COJ300 is shown in black plus (+) symbol for comparison. Pure SOA IN onset SS_i are presented as an asterisk (✳) symbol for each organic species, respectively. The solid blue and black lines are water saturation lines and homogeneous lines for 200 nm aqueous droplets (Koop et al., 2000), respectively. A representative temperature and SS_i error bar is given on the left side for each panel.

There exists no distinguishable difference between bare COJ300 and BC coated with highly oxidized toluene SOA (*T-10* in Table 2) from -46 to -44 °C. Ice crystals may form on the carbonaceous part of partially coated particles, whose IN onset SS_i should be the same as bare COJ300. At temperatures above -43 °C, toluene SOA-coated BC particles nucleate ice at SS_i ~0.1 to 0.15 above bare 350 nm COJ300, but still ~0.15 below the homogeneous freezing threshold. This is in agreement with Wang et al. (2012) that pure aromatic SOA nucleate ice at SS_i 0.1-0.15 below the homogeneous freezing limit. BC coated by ~10-15 equivalent days atmospherically oxidized toluene SOA (*T-3* in Table 2) particles nucleate ice in deposition mode at higher SS_i than highly oxidized toluene SOA-coated BC within the investigated temperature range. Previous studies reported a molar weight range of 58-135 g mol^{-1} for toluene SOA (e.g., Bohn, 2001; Ji et al., 2017). The toluene SOA mass spectrum in Fig. 6(a) exhibits higher m/z = 44 and lower m/z = 43 fraction signal, indicating more oxidized organic species were generated during *T-10* and *T-3* experiments (Lambe et al., 2011b), agreeing with the previous study on toluene SOA (Liu et al., 2018). On the one hand, the higher O/C ratio (Fig. 7) of toluene-derived SOA when compared with the other two types of SOA may enhance the hygroscopicity of the particle (Lambe et al., 2011b; Liu et al., 2018; Zhao et al., 2016) and thus may reduce the deposition IN ability of BC particles. On the other hand, Hinks et al. (2018) shows that toluene-derived SOA also contains a significant amount of oligomers under dry laboratory conditions, similar to what we conducted in the PAM chamber in this study, potentially reducing the hygroscopicity and altering the phase state of the SOA to be semi-solid or solid (Li et al., 2020; Zhang et al., 2018b), under which the SOA can still nucleate ice (Zhang et al., 2019c). Overall, these two competing factors make our toluene SOA coating IN onset move towards but not fully in the homogeneous freezing regime, agreeing with the results of Kulkarni et al. (2016).

https://doi.org/10.5194/acp-2020-809
Preprint. Discussion started: 2 September 2020

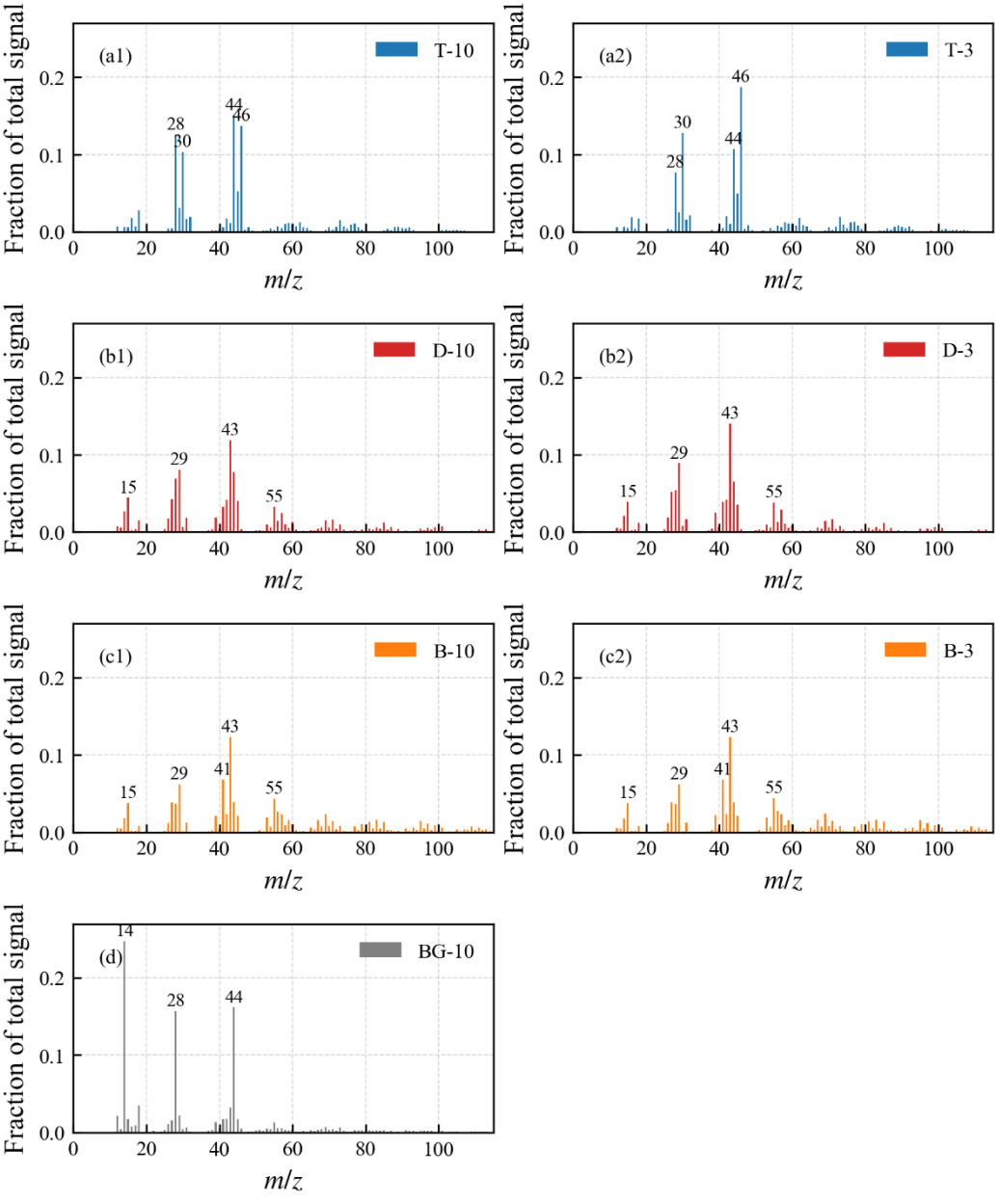

Figure 6. Normalized AMS mass spectra of COJ300 BC particles coated with (a) toluene SOA; (b) *n*-dodecane SOA; (c) *β*-caryophyllene SOA; and (d) bare COJ300 BC particles. More oxidized SOA is generated when toluene act as precursor, while less oxidized SOAs are generated when *n*-dodecane and *β*-caryophyllene act as precursors in this study, as indicated by the different fractions of *m/z* = 43 and 44, respectively (Canagaratna et al., 2015; Lambe et al., 2011b; Ng et al., 2011). The absolute organic mass loading present in the bare COJ300 BC experiment is less than 1% of the organic mass loading from the other three types of SOA coating experiments.

https://doi.org/10.5194/acp-2020-809
Preprint. Discussion started: 2 September 2020

Atmospheric Chemistry and Physics Discussions

IN onset SS_i of highly oxidized *n*-dodecane SOA-coated COJ300 particles (*D-10* in Table 2) in Fig. 5(b) nucleates ice homogeneously between -46 and -42 °C. BC coated by slightly oxidized *n*-dodecane SOA (*D-3* in Table 2) nucleates ice nominally lower than homogeneous freezing threshold between -43 and -40 °C. As shown in Fig. 5(c), the IN onset SS_i of OH-oxidized *β*-caryophyllene SOA-coated COJ300 particles (*B-10 and B-3* in Table 2) is in the homogeneous freezing regime. However, O_3 oxidized *β*-caryophyllene SOA shows no significantly alternation of IN ability. The mass spectra in Fig. 6(b) and Fig. 6(c) exhibit large fraction of signals at *m/z* = 15 (CH_3^+), 29 ($C_2H_5^+$), 43 ($C_3H_7^+$), and 55 ($C_4H_7^+$) for *n*-dodecane and *β*-caryophyllene SOA coating experiments in this study, implying formation of less oxidized aliphatic fragments during these experiments (Lambe et al., 2011b). The H/C and O/C values of *n*-dodecane and *β*-caryophyllene SOA coating in Fig. 7 are smaller than that of toluene SOA, which are in agreement with previous studies (Li et al., 2019; Pereira et al., 2019; Simonen et al., 2017). The slopes of H/C and O/C values of these two types of SOA and their respective two precursors (Fig. 7) are in the range between -1 and 0, which is consistent with the simultaneous formation of carboxylic acid functional groups and C-C bond breakage (Heald et al., 2010; Lambe et al., 2011b). Addition of carboxylic acid group may enhance the hygroscopicity of *n*-dodecane and *β*-caryophyllene SOA, and the hygroscopicity is further enhanced with more OH exposure (Bé et al., 2017; Frosch et al., 2013; Schilling et al., 2015; Yee et al., 2013). We conclude that BC with OH oxidized *n*-dodecane and *β*-caryophyllene SOA coatings, regardless of oxidation level, may condense on BC surface and forms organic films, leading to nucleation in the homogeneous regime.

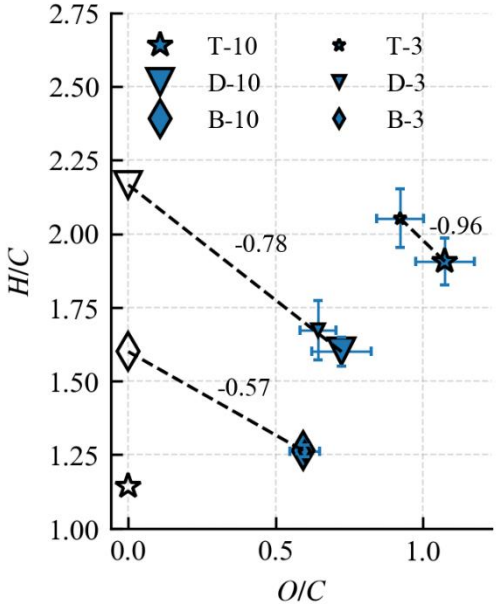

Figure 7. Elemental H/C ratio as a function of O/C ratio for three pure organic precursors (hollow symbols) and corresponding COJ300 BC particles seeded SOA inside the PAM reactor (filled symbols). Different symbol sizes denote different OH exposure level. The negative slopes SOA coating experiments are consistent with simultaneous carboxylic acid group addition and C-C single bond breakage (Heald et al., 2010; Lambe et al., 2011b).

https://doi.org/10.5194/acp-2020-809
Preprint. Discussion started: 2 September 2020


Atmospheric Chemistry and Physics Discussions

The experimental results are attributed to two factors: organic coating and volatility. Previous studies controlling the combustion fuel-air-ratio produced BC particles occupying different organic content fractions, with higher organic content resulting in amorphous organic surfaces (Crawford et al., 2011; Möhler et al., 2005b; Mahrt et al., 2018). Shifts from heterogeneous to homogeneous freezing with increasing organic content have been observed. Kulkarni et al. (2016) reported that α-pinene SOA coating suppressed the ice nucleation ability of BC particles. However, studies show that as the volatility of the organic coating decreases below certain threshold, especially near glass transition temperature, these organic coatings might be able to heterogeneously nucleate ice (Berkemeier et al., 2014; Murray et al., 2010; Zhang et al., 2019c). The suppression of BC IN ability by organic coating was attributed to coverage of surface-active sites and filling of pores on BC surface when the volatility of the organic coating is relatively high. Certain SOA coatings in this study are less oxidized and thus may similarly impair BC IN ability due to their relatively high volatility, as Docherty et al. (2018) and Hildebrandt Ruiz et al. (2015) showed an inverse correlation between the volatility and oxidation state. Our results suggest that less oxidized SOA (*n*-dodecane and β-caryophyllene derived SOA from photooxidation), despite their high mass loadings in PAM chamber, are more likely to condense on seed particle and forms fully coated BC particles, moving IN onset SS_i to the homogeneous regime, while β-caryophyllene SOA oxidized by O_3 did not alter the SS_i of the soot particles. In addition, more oxidized SOA (toluene derived SOA from photooxidation) with potentially more oligomer formation, moving IN onset SS_i towards, but still below, homogeneous freezing.

4 Atmospheric implications

BC particles emitted from combustion sources (such as aero-engines) are carbonaceous nanoscale fractal aggregates with primary particle diameter of 20-50 nm (Bockhorn et al., 2009; Vander Wal et al., 2014). These BC particles can remain suspend in the atmosphere for days, and might undergo compaction and atmospheric aging, such as oxidation and mixing with atmospheric aerosols. This study focuses on the impact of morphology, particle size and mixing state on the IN ability of BC-containing aerosols. Three BC proxies were chosen to represent freshly emitted (in other words, unoxidized and more fractal) BC (R2500U), unoxidized compacted BC (R330R), and atmospheric chemically aged BC (COJ300). The morphological characteristics, such as d_{pp}, circularity, roundness, and D_f, are within the value range of typical BC emitted from aircraft engines, vehicles, biomass burning, laboratory flames, and field observation (e.g., China et al., 2013; China et al., 2014; China et al., 2015; Lapuerta et al., 2007; Vander Wal et al., 2014; Zhang et al., 2019b). Findings in this study can be relevant to airborne aircraft emissions and ground emissions carried by updrafts to tropopause.

The IN results for bare BC particles show dependence on particle size and surface chemistry, but the role of fractal level seems to be of limited importance. The lower size limit of bare BC to exhibit IN activity is between 300-400 nm for R2500U at -46 °C. This is important for freshly emitted BC from aircraft engines and vehicles, which are usually fractal with d_m<200 nm (Kittelson, 1998; Moore et al., 2017). It is unlikely that small, freshly emitted BC will activate as INP in aircraft plumes

https://doi.org/10.5194/acp-2020-809
Preprint. Discussion started: 2 September 2020


Atmospheric Chemistry and Physics Discussions

below the homogeneous freezing threshold if they possess similar physicochemical properties as R2500U. The smallest size for compacted BC (R330R) to activate as INPs lies between 200-400 nm at -46 °C. This means that the IN ability of small BC particles may be enhanced after cloud cycles, during which fractal BC geometries may collapse and forms PCF favoring morphology (Mahrt et al., 2020). The COJ300 IN results imply that ice crystal formation may favor oxidized hydrophilic surfaces. The d_{pp} of COJ300 is appropriate for mesopores to accommodate ice crystal formation below water saturation. Particles down to 100 nm can act as efficient INP. This implies that for long-lived atmospheric BC particles, after being oxidized and compacted, may act as efficient INP.

To simulate atmospheric aging, toluene, *n*-dodecane and *β*-caryophyllene were chosen to represent anthropogenic and biogenic SOA precursors (Atkinson and Arey, 2003; Ding et al., 2014; Hu et al., 2008). Toluene-derived SOA coating impede BC heterogeneous IN activity slightly while *n*-dodecane and *β*-caryophyllene-derived SOA coatings caused BC particles to nucleate ice homogeneously. BC emitted from aircraft and vehicles are likely to be coated by toluene and *n*-dodecane derived SOA (e.g., Beyersdorf et al., 2012; Beyersdorf et al., 2014; Timko et al., 2014). According to our experimental results, even though such coating can facilitate particle growth, coated particles are more likely to nucleate ice near the homogeneous freezing threshold.

The conclusions drawn here for BC proxies may deviate from genuine BC collected from combustion sources. Nonetheless, BC surrogates are often used in research to mimic aircraft emitted BC for their similarity and availability (e.g., Persiantseva et al., 2004). Additional IN studies, over a wider temperature range would also be required for the proxies to firmly verify the PCF mechanism; the question whether the studied IN is depositional or in fact homogeneous IN of liquid water in pores and cavities, remains to be answered due to the limited temperature range investigated in this study.

5 Summary

The IN ability of size-selected (100-400 nm) monodisperse BC particles with different morphologies and surface chemistry and BC particles coated with toluene, *n*-dodecane, and *β*-caryophyllene-derived SOA has been systematically investigated in the cirrus temperature regime (-46 to -38 °C). Three aerosolized BC proxies were selected to represent particle morphology at different atmospheric aging stages, i.e. freshly emitted (R2500U), atmospheric compacted (R330R), and atmospheric oxidized (COJ300). The IN activity was investigated in relation to particle size, morphology, surface chemistry, SOA precursor type and OH exposure level.

The results show the lower size limit for BC particles to exhibit IN activity varies between BC type. 400 nm freshly emitted and compacted BC particles nucleate ice near the homogeneous freezing threshold. Ice crystals form on surface modified hydrophilic BC at SS_i as low as 1.15. The onset of some deposition nucleation, as opposed to purely homogeneous freezing, occurs for some BC types between 100-200 nm, in some cases below 100 nm. We conclude that BC IN favors larger

https://doi.org/10.5194/acp-2020-809
Preprint. Discussion started: 2 September 2020


Atmospheric Chemistry and Physics Discussions

particles and oxidized hydrophilic surface. The highly fractal BC particles did not necessarily act as superior deposition INP over more spherical ones as would normally be anticipated from surface active density theory. This might be caused by PCF occurring in the pores and cavities of more compacted particles.

Toluene-derived SOA coatings increase bare BC IN onset SS_i by 0.1-0.15, but still below the homogeneous freezing threshold. The larger molar weight of OH oxidized *n*-dodecane and *β*-caryophyllene SOA enhances the coating thickness and further elevates the IN onset SS_i into the homogeneous freezing regime. This might be due to SOA material filling the pores on BC surface and leading to IN near the homogeneous regime. O_3 oxidized *β*-caryophyllene SOA seems not to affect BC IN activity. OH exposure levels of all SOA coating experiments from 10-15 up to 90 equivalent atmospheric days shows no significant difference. Our study broadens aging processes of atmospheric BC particles and may offer the basis to better predict their IN activity and contribution to cirrus cloud formation. We suggest future studies should focus on IN activity of realistic combustion particles (aircraft, vehicles, and biomass burning, etc.) and advanced single particle characterization for validation of the PCF mechanism.

https://doi.org/10.5194/acp-2020-809
Preprint. Discussion started: 2 September 2020

Atmospheric Chemistry and Physics Discussions

Appendix A: BC morphology characterization

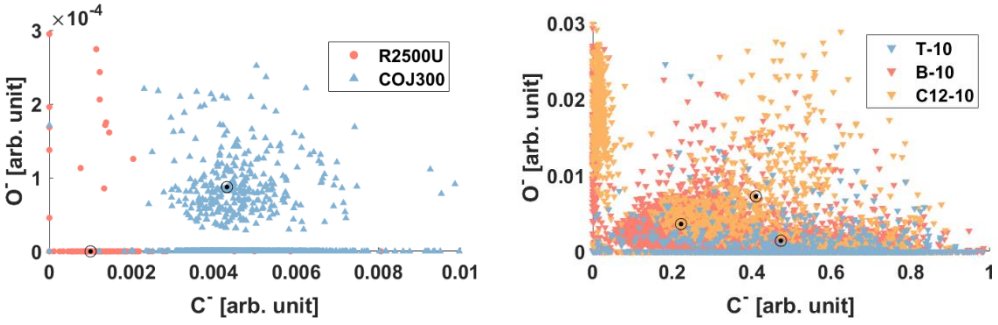

Figure A1. Negative polarity oxygen and carbon peak areas from PALMS for (left panel) 400 nm R2500U and COJ300 BC; (right panel) SOA-coated BC particles. Cluster centroid denoted as ⊙. Generally, COJ300 occupies a higher O^- signal than R2500U.

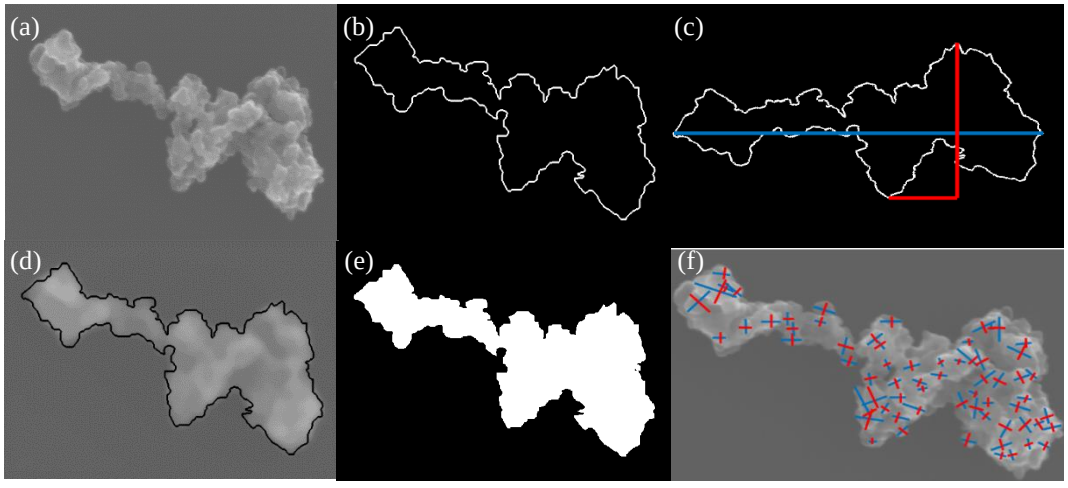

Figure A2. Example of processing of SEM images. (a) original image; (b) draw an approximate aggregate outline; (c) obtain the longest dimension (L_{max}) of an aggregate periphery to the perpendicular maximum width (W_{max}); (d) validation of the periphery; (e) use binary figure to obtain project aggregate area (A_a); (f) measurement of primary particle diameter (d_{pp}).

https://doi.org/10.5194/acp-2020-809
Preprint. Discussion started: 2 September 2020

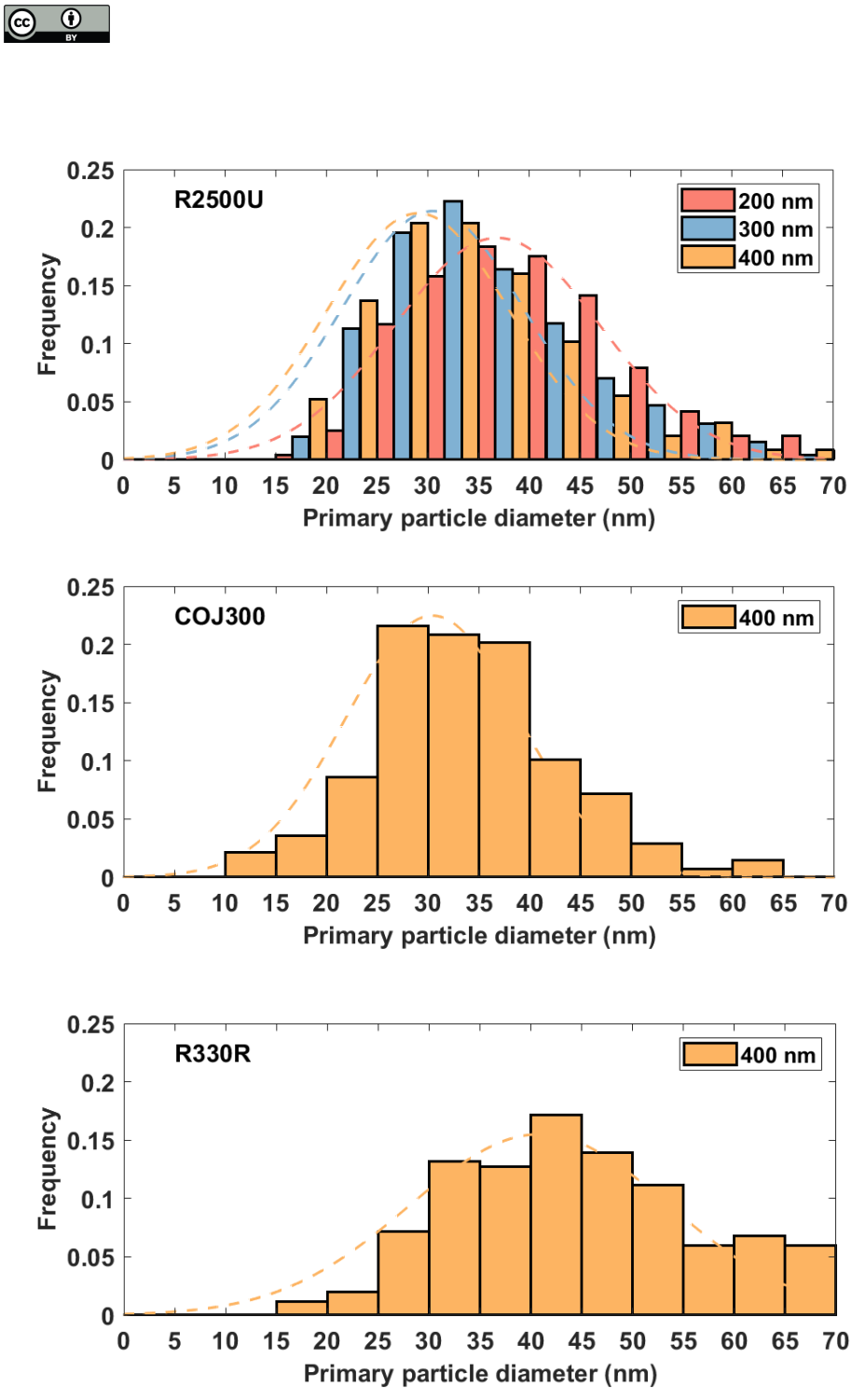

Figure A3. Primary particle size distributions for select BC particle types.

https://doi.org/10.5194/acp-2020-809
Preprint. Discussion started: 2 September 2020

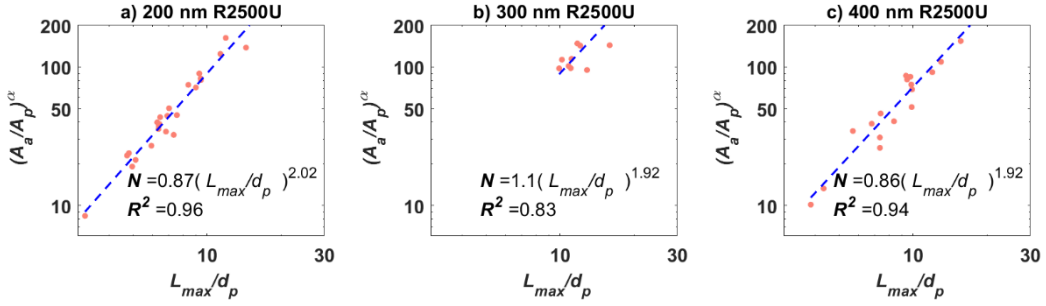

Figure A4. Power law fit to obtain 3-D fractal dimensions of (a) 200 nm (*N*=25), (b) 300 nm (*N*=12), (c) 400 nm (*N*=21) R2500U BC particles. More than 10 aggregates were analyzed for each size.

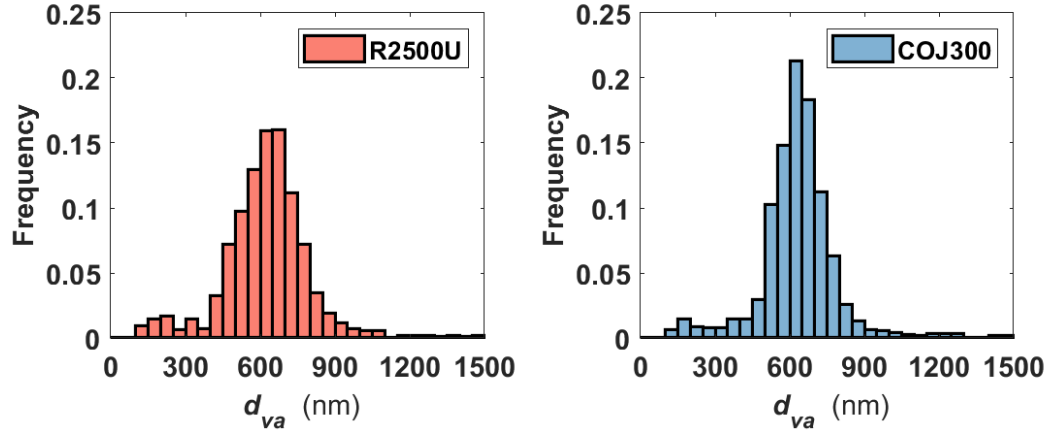

Figure A5. Vacuum aerodynamic diameter (d_{va}) derived from PALMS for 400 nm R2500U and COJ300 (Cziczo et al., 2006).

https://doi.org/10.5194/acp-2020-809
Preprint. Discussion started: 2 September 2020

Atmospheric Chemistry and Physics Discussions

Appendix B: SOA coating experiments

Table B1. Organic compounds engaged in this study. The parameters are taken from room temperature data.

Compound	Structure	Formula (m/z)	SOA mass yields (%)[a]	Rate constants×10^{12} [cm^3/(molecule·s)]	
Toluene		C_7H_8 (92)	8 - 49 (Hildebrandt et al., 2009)	k_{OH}	6.36 (Tully et al., 1981)
n-dodecane		$C_{12}H_{26}$ (170)	9 (Presto et al., 2010)	k_{OH}	13.3 (Lamkaddam et al., 2019)
β-caryophyllene	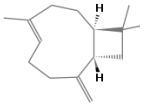	$C_{15}H_{24}$ (205)	17 - 63 (Griffin et al., 1999) 53[b] (Jaoui et al., 2013)	k_{OH} k_{zone}	200 (Atkinson and Arey, 2003 and reference therein) 1.16×10^{-2} (Shu and Atkinson, 1994)

[a]Measured at organic particle concentration of 10 µg/m^3; [b]Measured at organic particle concentration of 26 µg/m^3.

https://doi.org/10.5194/acp-2020-809
Preprint. Discussion started: 2 September 2020

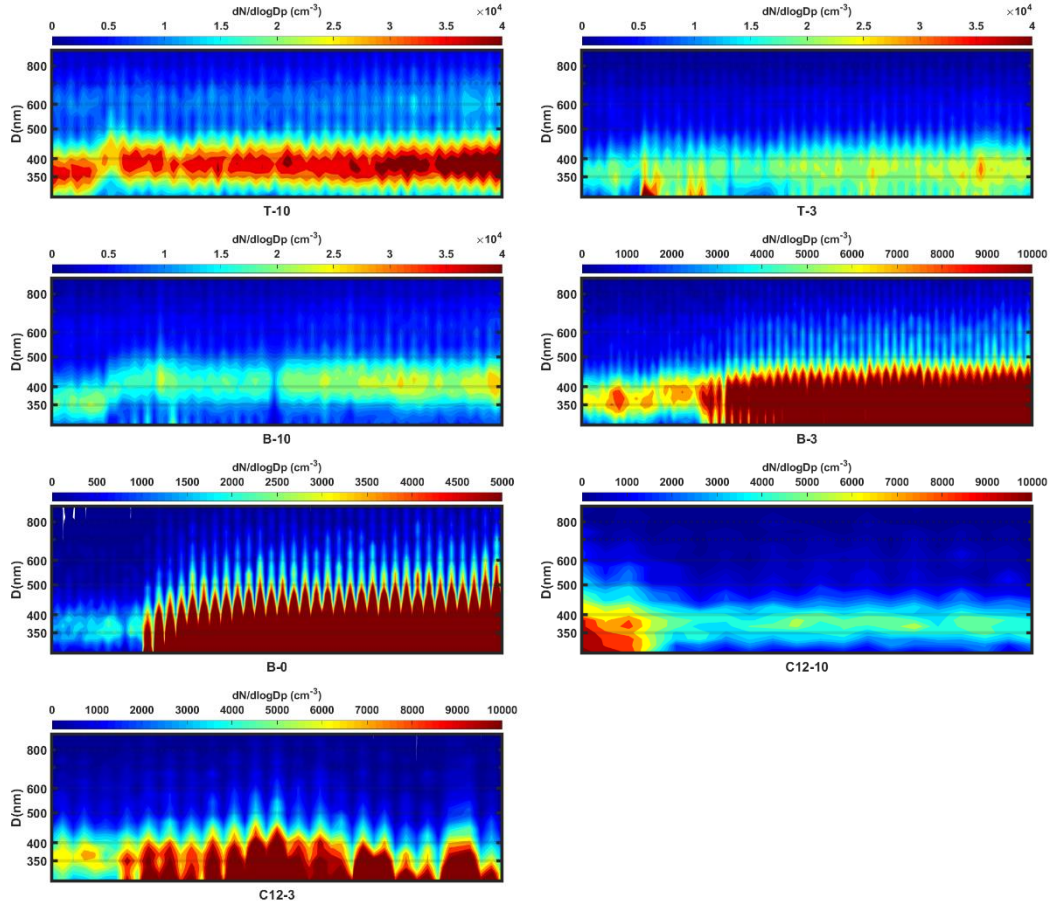

Figure B1. Particle size distribution for different BC and SOA mixing experiments. A size shift from 350 nm to 400 nm can be observed for each experiment.

https://doi.org/10.5194/acp-2020-809
Preprint. Discussion started: 2 September 2020

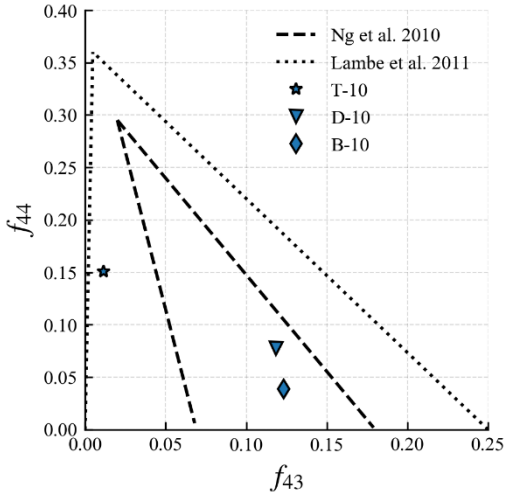

Figure B2. The measured fraction of AMS signals at *m/z* = 43 (f_{43}) and *m/z* = 44 (f_{44}). SOA generated from *n*-dodecane and *β*-caryophyllene in this study are within the ambient SOA f_{44} and f_{43} range measured by Ng et al. (2010). Toluene-derived SOA in this study exhibits similar f_{44} and f_{43} signal range to the laboratory measurement of glyoxal-derived SOA (Lambe et al., 2011b).

https://doi.org/10.5194/acp-2020-809
Preprint. Discussion started: 2 September 2020

Atmospheric Chemistry and Physics Discussions

Appendix C: Pressure drop due to the presence of pores and cavities

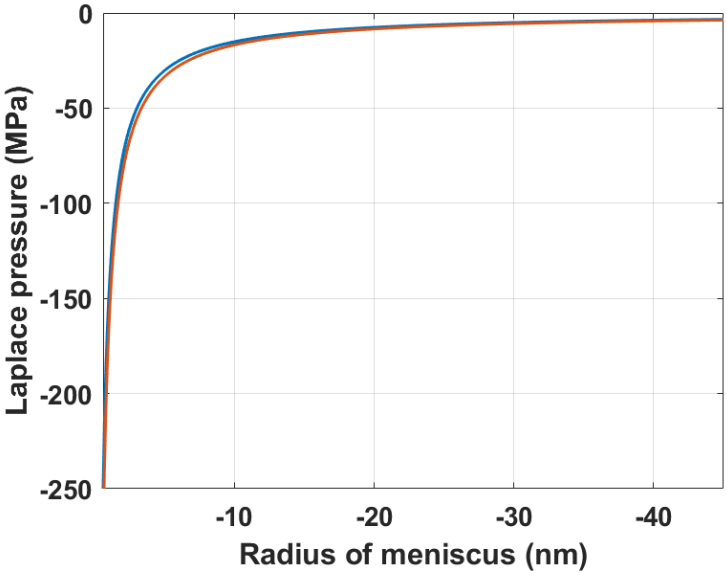

500 **Figure C1. Saturation pressure drop (Laplace pressure) as a function of the radius of the meniscus (Marcolli, 2020)**

https://doi.org/10.5194/acp-2020-809
Preprint. Discussion started: 2 September 2020

Author Contributions

CZ, YZ, MJW, LN, TBO and DJC designed the experiments and methodology. CZ collected black carbon samples and performed morphology characterization. CZ, YZ, MJW and CS performed chemical analyses, and measured ice nucleation activity. CZ, YZ, MJW, LN, LC, and DJC prepared manuscript with input from all coauthors.

Acknowledgments

The authors declare no competing interests. We thank Andrew Lambe and other colleagues at Aerodyne Research Inc. for their help with the PAM reactor and SOA coating experiment. This work was supported by National Natural Science Foundation of China (Grant No. 51922019) and Chinese Government Scholarship (Grant No. 201806020052). YZ was supported by the NSF Postdoctoral Fellowship under AGS Grant No. 1524731 and the National Institutes of Health (NIH) Grant No. T32ES007018.

https://doi.org/10.5194/acp-2020-809
Preprint. Discussion started: 2 September 2020

Atmospheric Chemistry and Physics Discussions

References

Alfarra, M. R., Hamilton, J. F., Wyche, K. P., Good, N., Ward, M. W., Carr, T., Barley, M. H., Monks, P. S., Jenkin, M. E., Lewis, A. C., and McFiggans, G. B.: The effect of photochemical ageing and initial precursor concentration on the composition and hygroscopic properties of β-caryophyllene secondary organic aerosol, Atmos. Chem. Phys., 12, 6417-6436, 10.5194/acp-12-6417-2012, 2012.

Anderson, B. E., Beyersdorf, A. J., Hudgins, C. H., Plant, J. V., Thornhill, K. L., Winstead, E. L., Ziemba, L. D., Howard, R., Corporan, E., Miake-Lye, R. C., Herndon, S. C., Timko, M., Woods, E., Dodds, W., Lee, B., Santoni, G., Whitefield, P., Hagen, D., Lobo, P., Knighton, W. B., Bulzan, D., Tacina, K., Wey, C., VanderWal, R., and Bhargava, A.: Alternative aviation fuel experiment (AAFEX), National Aeronautics and Space Administration, Langley Research Center. NASA/TM-2011-217059., Hanover, 2011.

Asa-Awuku, A., Engelhart, G. J., Lee, B. H., Pandis, S. N., and Nenes, A.: Relating CCN activity, volatility, and droplet growth kinetics of β-caryophyllene secondary organic aerosol, Atmos. Chem. Phys., 9, 795-812, 10.5194/acp-9-795-2009, 2009.

Atkinson, R., and Arey, J.: Gas-phase tropospheric chemistry of biogenic volatile organic compounds: a review, Atmospheric Environment, 37, 197-219, https://doi.org/10.1016/S1352-2310(03)00391-1, 2003.

Bé, A. G., Upshur, M. A., Liu, P., Martin, S. T., Geiger, F. M., and Thomson, R. J.: Cloud Activation Potentials for Atmospheric α-Pinene and β-Caryophyllene Ozonolysis Products, ACS Central Science, 3, 715-725, 10.1021/acscentsci.7b00112, 2017.

Berg, J. C.: Fluid Interfaces and Capillarity, in: An Introduction to Interfaces and Colloids: The Bridge to Nanoscience, World Scientific Publishing Co Pte Ltd., 23-106, 2009.

Berkemeier, T., Shiraiwa, M., Pöschl, U., and Koop, T.: Competition between water uptake and ice nucleation by glassy organic aerosol particles, Atmospheric Chemistry and Physics, 14, 12513-12531, 10.5194/acp-14-12513-2014, 2014.

Beyersdorf, A. J., Thornhill, K. L., Winstead, E. L., Ziemba, L. D., Blake, D. R., Timko, M. T., and Anderson, B. E.: Power-dependent speciation of volatile organic compounds in aircraft exhaust, Atmospheric Environment, 61, 275-282, https://doi.org/10.1016/j.atmosenv.2012.07.027, 2012.

Beyersdorf, A. J., Timko, M. T., Ziemba, L. D., Bulzan, D., Corporan, E., Herndon, S. C., Howard, R., Miake-Lye, R., Thornhill, K. L., Winstead, E., Wey, C., Yu, Z., and Anderson, B. E.: Reductions in aircraft particulate emissions due to the use of Fischer–Tropsch fuels, Atmospheric Chemistry and Physics, 14, 11-23, 10.5194/acp-14-11-2014, 2014.

Bikerman, J. J.: Capillarity before Laplace: Clairaut, Segner, Monge, Young, Archive for History of Exact Sciences, 18, 103-122, 10.1007/BF00348143, 1978.

Bockhorn, H., D'Anna, A., and Sarofim, A. F.: Combustion generated fine carbonaceous particles, edited by: Wang, H., Universitätsverlag Karlsruhe, Karlsruhe, 2009.

https://doi.org/10.5194/acp-2020-809
Preprint. Discussion started: 2 September 2020


Atmospheric Chemistry and Physics Discussions

545 Bohn, B.: Formation of Peroxy Radicals from OH−Toluene Adducts and O2, The Journal of Physical Chemistry A, 105, 6092-6101, 10.1021/jp0033972, 2001.

Bond, T. C., Streets, D. G., Yarber, K. F., Nelson, S. M., Woo, J.-H., and Klimont, Z.: A technology-based global inventory of black and organic carbon emissions from combustion, Journal of Geophysical Research: Atmospheres, 109, 10.1029/2003jd003697, 2004.

550 Bond, T. C., Doherty, S. J., Fahey, D. W., Forster, P. M., Berntsen, T., DeAngelo, B. J., Flanner, M. G., Ghan, S., Kärcher, B., Koch, D., Kinne, S., Kondo, Y., Quinn, P. K., Sarofim, M. C., Schultz, M. G., Schulz, M., Venkataraman, C., Zhang, H., Zhang, S., Bellouin, N., Guttikunda, S. K., Hopke, P. K., Jacobson, M. Z., Kaiser, J. W., Klimont, Z., Lohmann, U., Schwarz, J. P., Shindell, D., Storelvmo, T., Warren, S. G., and Zender, C. S.: Bounding the role of black carbon in the climate system: A scientific assessment, Journal of Geophysical Research: Atmospheres, 118, 5380-5552, 10.1002/jgrd.50171, 2013.

555 Brasil, A. M., Farias, T. L., and Carvalho, M. G.: A RECIPE FOR IMAGE CHARACTERIZATION OF FRACTAL-LIKE AGGREGATES, Journal of Aerosol Science, 30, 1379-1389, https://doi.org/10.1016/S0021-8502(99)00026-9, 1999.

Brooks, S. D., Suter, K., and Olivarez, L.: Effects of Chemical Aging on the Ice Nucleation Activity of Soot and Polycyclic Aromatic Hydrocarbon Aerosols, The Journal of Physical Chemistry A, 118, 10036-10047, 10.1021/jp508809y, 2014.

Burkhardt, U., and Kärcher, B.: Global radiative forcing from contrail cirrus, Nature Climate Change, 1, 54,
560 10.1038/nclimate1068, 2011.

Calogirou, A., Kotzias, D., and Kettrup, A.: Product analysis of the gas-phase reaction of β-caryophyllene with ozone, Atmospheric Environment, 31, 283-285, https://doi.org/10.1016/1352-2310(96)00190-2, 1997.

Canagaratna, M. R., Jimenez, J. L., J. H. Kroll, Chen, Q., Kessler, S. H., Massoli, P., Ruiz, L. H., Fortner, E., Williams, L. R., Wilson, K. R., Surratt, J. D., Donahue, N. M., Jayne, J. T., and Worsnop, D. R.: Elemental ratio measurements of organic
565 compounds using aerosol mass spectrometry: characterization, improved calibration, and implications, Atmospheric Chemistry and Physics, 253-272, 2015.

China, S., Mazzoleni, C., Gorkowski, K., Aiken, A. C., and Dubey, M. K.: Morphology and mixing state of individual freshly emitted wildfire carbonaceous particles, Nature communications, 4, 2122, 10.1038/ncomms3122, 2013.

China, S., Salvadori, N., and Mazzoleni, C.: Effect of Traffic and Driving Characteristics on Morphology of Atmospheric Soot
570 Particles at Freeway On-Ramps, Environmental science & technology, 48, 3128-3135, 10.1021/es405178n, 2014.

China, S., Scarnato, B., Owen, R. C., Zhang, B., Ampadu, M. T., Kumar, S., Dzepina, K., Dziobak, M. P., Fialho, P., Perlinger, J. A., Hueber, J., Helmig, D., Mazzoleni, L. R., and Mazzoleni, C.: Morphology and mixing state of aged soot particles at a remote marine free troposphere site: Implications for optical properties, Geophysical Research Letters, 42, 1243-1250, doi:10.1002/2014GL062404, 2015.

575 Chou, C., Kanji, Z. A., Stetzer, O., Tritscher, T., Chirico, R., Heringa, M. F., Weingartner, E., Prévôt, A. S. H., Baltensperger, U., and Lohmann, U.: Effect of photochemical ageing on the ice nucleation properties of diesel and wood burning particles, Atmos. Chem. Phys., 13, 761-772, 10.5194/acp-13-761-2013, 2013.

https://doi.org/10.5194/acp-2020-809
Preprint. Discussion started: 2 September 2020


Atmospheric Chemistry and Physics Discussions

Ciccioli, P., Brancaleoni, E., Frattoni, M., Di Palo, V., Valentini, R., Tirone, G., Seufert, G., Bertin, N., Hansen, U., Csiky, O., Lenz, R., and Sharma, M.: Emission of reactive terpene compounds from orange orchards and their removal by within-canopy processes, Journal of Geophysical Research: Atmospheres, 104, 8077-8094, 10.1029/1998jd100026, 1999.

Crawford, I., Möhler, O., Schnaiter, M., Saathoff, H., Liu, D., McMeeking, G., Linke, C., Flynn, M., Bower, K. N., Connolly, P. J., Gallagher, M. W., and Coe, H.: Studies of propane flame soot acting as heterogeneous ice nuclei in conjunction with single particle soot photometer measurements, Atmospheric Chemistry and Physics, 11, 9549-9561, 10.5194/acp-11-9549-2011, 2011.

Cziczo, D. J., Thomson, D. S., Thompson, T. L., DeMott, P. J., and Murphy, D. M.: Particle analysis by laser mass spectrometry (PALMS) studies of ice nuclei and other low number density particles, International Journal of Mass Spectrometry, 258, 21-29, 10.1016/j.ijms.2006.05.013, 2006.

David, R. O., Marcolli, C., Fahrni, J., Qiu, Y., Perez Sirkin, Y. A., Molinero, V., Mahrt, F., Brühwiler, D., Lohmann, U., and Kanji, Z. A.: Pore condensation and freezing is responsible for ice formation below water saturation for porous particles, Proceedings of the National Academy of Sciences, 116, 8184-8189, 10.1073/pnas.1813647116, 2019.

DeMott, P. J., Chen, Y., Kreidenweis, S. M., Rogers, D. C., and Sherman, D. E.: Ice formation by black carbon particles, Geophysical Research Letters, 26, 2429-2432, doi:10.1029/1999GL900580, 1999.

DeMott, P. J., Cziczo, D. J., Prenni, A. J., Murphy, D. M., Kreidenweis, S. M., Thomson, D. S., Borys, R., and Rogers, D. C.: Measurements of the concentration and composition of nuclei for cirrus formation, Proceedings of the National Academy of Sciences, 100, 14655-14660, 10.1073/pnas.2532677100, 2003.

Diehl, K., and Mitra, S. K.: A laboratory study of the effects of a kerosene-burner exhaust on ice nucleation and the evaporation rate of ice crystals, Atmospheric Environment, 32, 3145-3151, https://doi.org/10.1016/S1352-2310(97)00467-6, 1998.

Ding, X., He, Q.-F., Shen, R.-Q., Yu, Q.-Q., and Wang, X.-M.: Spatial distributions of secondary organic aerosols from isoprene, monoterpenes, β-caryophyllene, and aromatics over China during summer, Journal of Geophysical Research: Atmospheres, 119, 11,877-811,891, 10.1002/2014jd021748, 2014.

Docherty, K. S., Corse, E. W., Jaoui, M., Offenberg, J. H., Kleindienst, T. E., Krug, J. D., Riedel, T. P., and Lewandowski, M.: Trends in the oxidation and relative volatility of chamber-generated secondary organic aerosol, Aerosol Science and Technology, 52, 992-1004, 10.1080/02786826.2018.1500014, 2018.

Dooley, S., Won, S. H., Chaos, M., Heyne, J., Ju, Y., Dryer, F. L., Kumar, K., Sung, C.-J., Wang, H., Oehlschlaeger, M. A., Santoro, R. J., and Litzinger, T. A.: A jet fuel surrogate formulated by real fuel properties, Combustion and Flame, 157, 2333-2339, https://doi.org/10.1016/j.combustflame.2010.07.001, 2010.

Dooley, S., Won, S. H., Jahangirian, S., Ju, Y., Dryer, F. L., Wang, H., and Oehlschlaeger, M. A.: The combustion kinetics of a synthetic paraffinic jet aviation fuel and a fundamentally formulated, experimentally validated surrogate fuel, Combustion and Flame, 159, 3014-3020, 10.1016/j.combustflame.2012.04.010, 2012.

610 Dymarska, M., Murray, B. J., Sun, L., Eastwood, M. L., Knopf, D. A., and Bertram, A. K.: Deposition ice nucleation on soot at temperatures relevant for the lower troposphere, Journal of Geophysical Research: Atmospheres, 111, doi:10.1029/2005JD006627, 2006.

Fornea, A. P., Brooks, S. D., Dooley, J. B., and Saha, A.: Heterogeneous freezing of ice on atmospheric aerosols containing ash, soot, and soil, Journal of Geophysical Research: Atmospheres, 114, doi:10.1029/2009JD011958, 2009.

615 Friedman, B., Kulkarni, G., Beránek, J., Zelenyuk, A., Thornton, J. A., and Cziczo, D. J.: Ice nucleation and droplet formation by bare and coated soot particles, Journal of Geophysical Research, 116, 10.1029/2011jd015999, 2011.

Frosch, M., Bilde, M., Nenes, A., Praplan, A. P., Jurányi, Z., Dommen, J., Gysel, M., Weingartner, E., and Baltensperger, U.: CCN activity and volatility of β-caryophyllene secondary organic aerosol, Atmos. Chem. Phys., 13, 2283-2297, 10.5194/acp-13-2283-2013, 2013.

620 Fu, H., Zhang, M., Li, W., Chen, J., Wang, L., Quan, X., and Wang, W.: Morphology, composition and mixing state of individual carbonaceous aerosol in urban Shanghai, Atmos. Chem. Phys., 12, 693-707, 10.5194/acp-12-693-2012, 2012.

Garimella, S., Kristensen, T. B., Ignatius, K., Welti, A., Voigtländer, J., Kulkarni, G. R., Sagan, F., Kok, G. L., Dorsey, J., Nichman, L., Rothenberg, D. A., Rösch, M., Kirchgäßner, A. C. R., Ladkin, R., Wex, H., Wilson, T. W., Ladino, L. A., Abbatt, J. P. D., Stetzer, O., Lohmann, U., Stratmann, F., and Cziczo, D. J.: The SPectrometer for Ice Nuclei (SPIN): an

625 instrument to investigate ice nucleation, Atmospheric Measurement Techniques, 9, 2781-2795, 10.5194/amt-9-2781-2016, 2016.

Garimella, S., Rothenberg, D. A., Wolf, M. J., David, R. O., Kanji, Z. A., Wang, C., Rösch, M., and Cziczo, D. J.: Uncertainty in counting ice nucleating particles with continuous flow diffusion chambers, Atmos. Chem. Phys., 17, 10855-10864, 10.5194/acp-17-10855-2017, 2017.

630 Griffin, R. J., Cocker III, D. R., Seinfeld, J. H., and Dabdub, D.: Estimate of global atmospheric organic aerosol from oxidation of biogenic hydrocarbons, Geophysical Research Letters, 26, 2721-2724, 10.1029/1999gl900476, 1999.

Guenther, A. B., Jiang, X., Heald, C. L., Sakulyanontvittaya, T., Duhl, T., Emmons, L. K., and Wang, X.: The Model of Emissions of Gases and Aerosols from Nature version 2.1 (MEGAN2.1): an extended and updated framework for modeling biogenic emissions, Geosci. Model Dev., 5, 1471-1492, 10.5194/gmd-5-1471-2012, 2012.

635 Heald, C. L., Kroll, J. H., Jimenez, J. L., Docherty, K. S., DeCarlo, P. F., Aiken, A. C., Chen, Q., Martin, S. T., Farmer, D. K., and Artaxo, P.: A simplified description of the evolution of organic aerosol composition in the atmosphere, Geophysical Research Letters, 37, 10.1029/2010gl042737, 2010.

Henrot, A. J., Stanelle, T., Schröder, S., Siegenthaler, C., Taraborrelli, D., and Schultz, M. G.: Implementation of the MEGAN (v2.1) biogenic emission model in the ECHAM6-HAMMOZ chemistry climate model, Geosci. Model Dev., 10, 903-926,

640 10.5194/gmd-10-903-2017, 2017.

Heymsfield, A. J., Krämer, M., Luebke, A., Brown, P., Cziczo, D. J., Franklin, C., Lawson, P., Lohmann, U., McFarquhar, G., Ulanowski, Z., and Van Tricht, K.: Cirrus Clouds, Meteorological Monographs, 58, 2.1-2.26, 10.1175/amsmonographs-d-16-0010.1, 2017.

https://doi.org/10.5194/acp-2020-809
Preprint. Discussion started: 2 September 2020


Atmospheric Chemistry and Physics Discussions

Hildebrandt, L., Donahue, N. M., and Pandis, S. N.: High formation of secondary organic aerosol from the photo-oxidation of toluene, Atmos. Chem. Phys., 9, 2973-2986, 10.5194/acp-9-2973-2009, 2009.

Hildebrandt Ruiz, L., Paciga, A. L., Cerully, K. M., Nenes, A., Donahue, N. M., and Pandis, S. N.: Formation and aging of secondary organic aerosol from toluene: changes in chemical composition, volatility, and hygroscopicity, Atmos. Chem. Phys., 15, 8301-8313, 10.5194/acp-15-8301-2015, 2015.

Hinks, M. L., Montoya-Aguilera, J., Ellison, L., Lin, P., Laskin, A., Laskin, J., Shiraiwa, M., Dabdub, D., and Nizkorodov, S. A.: Effect of relative humidity on the composition of secondary organic aerosol from the oxidation of toluene, Atmos. Chem. Phys., 18, 1643-1652, 10.5194/acp-18-1643-2018, 2018.

Hoffmann, T., Odum, J. R., Bowman, F., Collins, D., Klockow, D., Flagan, R. C., and Seinfeld, J. H.: Formation of Organic Aerosols from the Oxidation of Biogenic Hydrocarbons, Journal of Atmospheric Chemistry, 26, 189-222, 10.1023/A:1005734301837, 1997.

Hoose, C., and Möhler, O.: Heterogeneous ice nucleation on atmospheric aerosols: a review of results from laboratory experiments, Atmospheric Chemistry and Physics, 12, 9817-9854, 10.5194/acp-12-9817-2012, 2012.

Hu, D., Bian, Q., Li, T. W. Y., Lau, A. K. H., and Yu, J. Z.: Contributions of isoprene, monoterpenes, β-caryophyllene, and toluene to secondary organic aerosols in Hong Kong during the summer of 2006, Journal of Geophysical Research: Atmospheres, 113, 10.1029/2008jd010437, 2008.

IPCC: IPCC, 2013: Climate Change 2013: The Physical Science Basis. Contribution of Working Group I to the Fifth Assessment Report of the Intergovernmental Panel on Climate Change [Stocker, T.F., D. Qin, G.-K. Plattner, M. Tignor, S.K. Allen, J. Boschung, A. Nauels, Y. Xia, V. Bex and P.M. Midgley (eds.)]. Cambridge University Press, Cambridge, United Kingdom and New York, NY, USA., 2013.

Jaoui, M., Kleindienst, T. E., Docherty, K. S., Lewandowski, M., and Offenberg, J. H.: Secondary organic aerosol formation from the oxidation of a series of sesquiterpenes: α-cedrene, β-caryophyllene, α-humulene and α-farnesene with O3, OH and NO3 radicals, Environmental Chemistry, 10, 178-193, https://doi.org/10.1071/EN13025, 2013.

Jayne, J. T., Leard, D. C., Zhang, X., Davidovits, P., Smith, K. A., Kolb, C. E., and Worsnop, D. R.: Development of an Aerosol Mass Spectrometer for Size and Composition Analysis of Submicron Particles, Aerosol Science and Technology, 33, 49-70, 10.1080/027868200410840, 2000.

Ji, Y., Zhao, J., Terazono, H., Misawa, K., Levitt, N. P., Li, Y., Lin, Y., Peng, J., Wang, Y., Duan, L., Pan, B., Zhang, F., Feng, X., An, T., Marrero-Ortiz, W., Secrest, J., Zhang, A. L., Shibuya, K., Molina, M. J., and Zhang, R.: Reassessing the atmospheric oxidation mechanism of toluene, Proceedings of the National Academy of Sciences, 114, 8169-8174, 10.1073/pnas.1705463114, 2017.

Kärcher, B., Möhler, O., DeMott, P. J., Pechtl, S., and Yu, F.: Insights into the role of soot aerosols in cirrus cloud formation, Atmos. Chem. Phys., 7, 4203-4227, 10.5194/acp-7-4203-2007, 2007.

Kärcher, B.: Formation and radiative forcing of contrail cirrus, Nature communications, 9, 1824, 10.1038/s41467-018-04068-0, 2018.

https://doi.org/10.5194/acp-2020-809
Preprint. Discussion started: 2 September 2020


Atmospheric Chemistry and Physics Discussions

Köylü, Ü. Ö., Faeth, G. M., Farias, T. L., and Carvalho, M. G.: Fractal and projected structure properties of soot aggregates, Combustion and Flame, 100, 621-633, https://doi.org/10.1016/0010-2180(94)00147-K, 1995.

Kang, E., Root, M. J., Toohey, D. W., and Brune, W. H.: Introducing the concept of Potential Aerosol Mass (PAM), Atmos. Chem. Phys., 7, 5727-5744, 10.5194/acp-7-5727-2007, 2007.

Kanji, Z. A., and Abbatt, J. P. D.: Laboratory studies of ice formation via deposition mode nucleation onto mineral dust and n-hexane soot samples, Journal of Geophysical Research, 111, 10.1029/2005jd006766, 2006.

Kanji, Z. A., DeMott, P. J., Möhler, O., and Abbatt, J. P. D.: Results from the University of Toronto continuous flow diffusion chamber at ICIS 2007: instrument intercomparison and ice onsets for different aerosol types, Atmospheric Chemistry and Physics, 11, 31-41, 10.5194/acp-11-31-2011, 2011.

Kanji, Z. A., Ladino, L. A., Wex, H., Boose, Y., Burkert-Kohn, M., Cziczo, D. J., and Krämer, M.: Overview of Ice Nucleating Particles, Meteorological Monographs, 58, 1.1-1.33, 10.1175/amsmonographs-d-16-0006.1, 2017.

Kinsey, J. S., Dong, Y., Williams, D. C., and Logan, R.: Physical characterization of the fine particle emissions from commercial aircraft engines during the Aircraft Particle Emissions eXperiment (APEX) 1–3, Atmospheric Environment, 44, 2147-2156, 10.1016/j.atmosenv.2010.02.010, 2010.

Kinsey, J. S., Hays, M. D., Dong, Y., Williams, D. C., and Logan, R.: Chemical characterization of the fine particle emissions from commercial aircraft engines during the Aircraft Particle Emissions eXperiment (APEX) 1 to 3, Environmental science & technology, 45, 3415-3421, 10.1021/es103880d, 2011.

Kittelson, D. B.: Engines and nanoparticles: a review, Journal of Aerosol Science, 29, 575-588, https://doi.org/10.1016/S0021-8502(97)10037-4, 1998.

Koehler, K. A., DeMott, P. J., Kreidenweis, S. M., Popovicheva, O. B., Petters, M. D., Carrico, C. M., Kireeva, E. D., Khokhlova, T. D., and Shonija, N. K.: Cloud condensation nuclei and ice nucleation activity of hydrophobic and hydrophilic soot particles, Physical Chemistry Chemical Physics, 11, 7906-7920, 10.1039/B905334B, 2009.

Koop, T., Luo, B., Tsias, A., and Peter, T.: Water activity as the determinant for homogeneous ice nucleation in aqueous solutions, Nature, 406, 611, 10.1038/35020537, 2000.

Koop, T.: Crystals creeping out of cracks, Proceedings of the National Academy of Sciences, 114, 797-799, 10.1073/pnas.1620084114, 2017.

Kulkarni, G., China, S., Liu, S., Nandasiri, M., Sharma, N., Wilson, J., Aiken, A. C., Chand, D., Laskin, A., Mazzoleni, C., Pekour, M., Shilling, J., Shutthanandan, V., Zelenyuk, A., and Zaveri, R. A.: Ice nucleation activity of diesel soot particles at cirrus relevant temperature conditions: Effects of hydration, secondary organics coating, soot morphology, and coagulation, Geophysical Research Letters, 43, 3580-3588, 10.1002/2016gl068707, 2016.

Kulkarni, G. R., and Kok, G. L.: Mobile Ice Nucleus Spectrometer, ; Pacific Northwest National Lab. (PNNL), Richland, WA (United States)PNNL-21384; Other: 600306000 United States 10.2172/1071991 Other: 600306000 PNNL English, Medium: ED; Size: PDFN, 2012.

https://doi.org/10.5194/acp-2020-809
Preprint. Discussion started: 2 September 2020

Kumfer, B., and Kennedy, I.: The role of soot in the health effects of inhaled airborne particles, Combustion generated fine carbonaceous particles, edited by: Bockhorn, H., D'Anna, A., Sarofim, A. F., and Wang, H., Universitätsverlag Karlsruhe, Karlsruhe, 720 pp., 2009.

Lambe, A. T., Ahern, A. T., Williams, L. R., Slowik, J. G., Wong, J. P. S., Abbatt, J. P. D., Brune, W. H., Ng, N. L., Wright, J. P., Croasdale, D. R., Worsnop, D. R., Davidovits, P., and Onasch, T. B.: Characterization of aerosol photooxidation flow reactors: heterogeneous oxidation, secondary organic aerosol formation and cloud condensation nuclei activity measurements, Atmos. Meas. Tech., 4, 445-461, 10.5194/amt-4-445-2011, 2011a.

Lambe, A. T., Onasch, T. B., Massoli, P., Croasdale, D. R., Wright, J. P., Ahern, A. T., Williams, L. R., Worsnop, D. R., Brune, W. H., and Davidovits, P.: Laboratory studies of the chemical composition and cloud condensation nuclei (CCN) activity of secondary organic aerosol (SOA) and oxidized primary organic aerosol (OPOA), Atmos. Chem. Phys., 11, 8913-8928, 10.5194/acp-11-8913-2011, 2011b.

Lamkaddam, H., Gratien, A., Ropion, M., Pangui, E., and Doussin, J.-F.: Kinetic Study of the Temperature Dependence of OH-Initiated Oxidation of n-Dodecane, The Journal of Physical Chemistry A, 123, 9462-9468, 10.1021/acs.jpca.9b07704, 2019.

Lapuerta, M., Martos, F. J., and Herreros, J. M.: Effect of engine operating conditions on the size of primary particles composing diesel soot agglomerates, Journal of Aerosol Science, 38, 455-466, https://doi.org/10.1016/j.jaerosci.2007.02.001, 2007.

Lee, A., Goldstein, A. H., Kroll, J. H., Ng, N. L., Varutbangkul, V., Flagan, R. C., and Seinfeld, J. H.: Gas-phase products and secondary aerosol yields from the photooxidation of 16 different terpenes, Journal of Geophysical Research: Atmospheres, 111, 10.1029/2006jd007050, 2006.

Lee, C., and Kramer, T. A.: Prediction of three-dimensional fractal dimensions using the two-dimensional properties of fractal aggregates, Advances in Colloid and Interface Science, 112, 49-57, https://doi.org/10.1016/j.cis.2004.07.001, 2004.

Lee, D. S., Fahey, D. W., Forster, P. M., Newton, P. J., Wit, R. C. N., Lim, L. L., Owen, B., and Sausen, R.: Aviation and global climate change in the 21st century, Atmospheric Environment, 43, 3520-3537, 10.1016/j.atmosenv.2009.04.024, 2009.

Lee, D. S., Pitari, G., Grewe, V., Gierens, K., Penner, J. E., Petzold, A., Prather, M. J., Schumann, U., Bais, A., Berntsen, T., Iachetti, D., Lim, L. L., and Sausen, R.: Transport impacts on atmosphere and climate: Aviation, Atmospheric Environment, 44, 4678-4734, https://doi.org/10.1016/j.atmosenv.2009.06.005, 2010.

Lefebvre, A. H.: Gas turbine combustion, CRC press, 1998.

Li, K., Chen, L., Han, K., Lv, B., Bao, K., Wu, X., Gao, X., and Cen, K.: Smog chamber study on aging of combustion soot in isoprene/SO2/NOx system: Changes of mass, size, effective density, morphology and mixing state, Atmospheric Research, 184, 139-148, https://doi.org/10.1016/j.atmosres.2016.10.011, 2017.

Li, K., Liggio, J., Lee, P., Han, C., Liu, Q., and Li, S. M.: Secondary organic aerosol formation from α-pinene, alkanes, and oil-sands-related precursors in a new oxidation flow reactor, Atmos. Chem. Phys., 19, 9715-9731, 10.5194/acp-19-9715-2019, 2019.

Li, W., Shao, L., Zhang, D., Ro, C.-U., Hu, M., Bi, X., Geng, H., Matsuki, A., Niu, H., and Chen, J.: A review of single aerosol particle studies in the atmosphere of East Asia: morphology, mixing state, source, and heterogeneous reactions, Journal of Cleaner Production, 112, 1330-1349, https://doi.org/10.1016/j.jclepro.2015.04.050, 2016.

Li, Y., Day, D. A., Stark, H., Jimenez, J. L., and Shiraiwa, M.: Predictions of the glass transition temperature and viscosity of organic aerosols from volatility distributions, Atmos. Chem. Phys., 20, 8103-8122, 10.5194/acp-20-8103-2020, 2020.

Liati, A., Brem, B. T., Durdina, L., Vogtli, M., Dasilva, Y. A., Eggenschwiler, P. D., and Wang, J.: Electron microscopic study of soot particulate matter emissions from aircraft turbine engines, Environmental science & technology, 48, 10975-10983, 10.1021/es501809b, 2014.

Liu, H., and Cao, G.: Effectiveness of the Young-Laplace equation at nanoscale, Scientific Reports, 6, 23936, 10.1038/srep23936, 2016.

Liu, T., Huang, D. D., Li, Z., Liu, Q., Chan, M., and Chan, C. K.: Comparison of secondary organic aerosol formation from toluene on initially wet and dry ammonium sulfate particles at moderate relative humidity, Atmos. Chem. Phys., 18, 5677-5689, 10.5194/acp-18-5677-2018, 2018.

Lobo, P., Durdina, L., Smallwood, G. J., Rindlisbacher, T., Siegerist, F., Black, E. A., Yu, Z., Mensah, A. A., Hagen, D. E., Miake-Lye, R. C., Thomson, K. A., Brem, B. T., Corbin, J. C., Abegglen, M., Sierau, B., Whitefield, P. D., and Wang, J.: Measurement of Aircraft Engine Non-Volatile PM Emissions: Results of the Aviation-Particle Regulatory Instrumentation Demonstration Experiment (A-PRIDE) 4 Campaign, Aerosol Science and Technology, 49, 472-484, 10.1080/02786826.2015.1047012, 2015.

Loza, C. L., Craven, J. S., Yee, L. D., Coggon, M. M., Schwantes, R. H., Shiraiwa, M., Zhang, X., Schilling, K. A., Ng, N. L., Canagaratna, M. R., Ziemann, P. J., Flagan, R. C., and Seinfeld, J. H.: Secondary organic aerosol yields of 12-carbon alkanes, Atmos. Chem. Phys., 14, 1423-1439, 10.5194/acp-14-1423-2014, 2014.

Möhler, O., Büttner, S., Linke, C., Schnaiter, M., Saathoff, H., Stetzer, O., Wagner, R., Krämer, M., Mangold, A., Ebert, V., and Schurath, U.: Effect of sulfuric acid coating on heterogeneous ice nucleation by soot aerosol particles, Journal of Geophysical Research: Atmospheres, 110, doi:10.1029/2004JD005169, 2005a.

Möhler, O., Linke, C., Saathoff, H., Schnaiter, M., Wagner, R., Mangold, A., Krämer, M., and Schurath, U.: Ice nucleation on flame soot aerosol of different organic carbon content, Meteorologische Zeitschrift, 14, 477-484, 10.1127/0941-2948/2005/0055, 2005b.

Mahrt, F., Marcolli, C., David, R. O., Gronquist, P., Meier, E. J. B., Lohmann, U., and Kanji, Z. A.: Ice nucleation abilities of soot particles determined with the Horizontal Ice Nucleation Chamber, Atmospheric Chemistry and Physics, 18, 13363-13392, 10.5194/acp-18-13363-2018, 2018.

https://doi.org/10.5194/acp-2020-809
Preprint. Discussion started: 2 September 2020


Atmospheric Chemistry and Physics Discussions

Mahrt, F., Kilchhofer, K., Marcolli, C., Grönquist, P., David, R. O., Rösch, M., Lohmann, U., and Kanji, Z. A.: The Impact of Cloud Processing on the Ice Nucleation Abilities of Soot Particles at Cirrus Temperatures, Journal of Geophysical Research: Atmospheres, 125, e2019JD030922, 10.1029/2019jd030922, 2020.

Mandelbrot, B. B.: The Fractal Geometry of Nature, W. H. Freeman and Company, San Francisco, 1982.

Marcolli, C.: Deposition nucleation viewed as homogeneous or immersion freezing in pores and cavities, Atmospheric Chemistry and Physics, 14, 2071-2104, 10.5194/acp-14-2071-2014, 2014.

Marcolli, C.: Pre-activation of aerosol particles by ice preserved in pores, Atmos. Chem. Phys., 17, 1595-1622, 10.5194/acp-17-1595-2017, 2017.

Marcolli, C.: Technical note: Fundamental aspects of ice nucleation via pore condensation and freezing including Laplace pressure and growth into macroscopic ice, Atmos. Chem. Phys., 20, 3209-3230, 10.5194/acp-20-3209-2020, 2020.

Moffet, R. C., O'Brien, R. E., Alpert, P. A., Kelly, S. T., Pham, D. Q., Gilles, M. K., Knopf, D. A., and Laskin, A.: Morphology and mixing of black carbon particles collected in central California during the CARES field study, Atmos. Chem. Phys., 16, 14515-14525, 10.5194/acp-16-14515-2016, 2016.

Moore, R. H., Thornhill, K. L., Weinzierl, B., Sauer, D., D'Ascoli, E., Kim, J., Lichtenstern, M., Scheibe, M., Beaton, B., Beyersdorf, A. J., Barrick, J., Bulzan, D., Corr, C. A., Crosbie, E., Jurkat, T., Martin, R., Riddick, D., Shook, M., Slover, G., Voigt, C., White, R., Winstead, E., Yasky, R., Ziemba, L. D., Brown, A., Schlager, H., and Anderson, B. E.: Biofuel blending reduces particle emissions from aircraft engines at cruise conditions, Nature, 543, 411-415, 10.1038/nature21420, 2017.

Murphy, D. M., Thomson, D. S., Middlebrook, A. M., and Schein, M. E.: In situ single-particle characterization at Cape Grim, Journal of Geophysical Research: Atmospheres, 103, 16485-16491, 10.1029/97JD03281, 1998.

Murray, B. J., Wilson, T. W., Dobbie, S., Cui, Z., Al-Jumur, S. M. R. K., Möhler, O., Schnaiter, M., Wagner, R., Benz, S., Niemand, M., Saathoff, H., Ebert, V., Wagner, S., and Kärcher, B.: Heterogeneous nucleation of ice particles on glassy aerosols under cirrus conditions, Nature Geoscience, 3, 233-237, 10.1038/ngeo817, 2010.

Ng, N. L., Canagaratna, M. R., Zhang, Q., Jimenez, J. L., Tian, J., Ulbrich, I. M., Kroll, J. H., Docherty, K. S., Chhabra, P. S., Bahreini, R., Murphy, S. M., Seinfeld, J. H., Hildebrandt, L., Donahue, N. M., DeCarlo, P. F., Lanz, V. A., Prévôt, A. S. H., Dinar, E., Rudich, Y., and Worsnop, D. R.: Organic aerosol components observed in Northern Hemispheric datasets from Aerosol Mass Spectrometry, Atmos. Chem. Phys., 10, 4625-4641, 10.5194/acp-10-4625-2010, 2010.

Ng, N. L., Canagaratna, M. R., Jimenez, J. L., Chhabra, P. S., Seinfeld, J. H., and Worsnop, D. R.: Changes in organic aerosol composition with aging inferred from aerosol mass spectra, Atmos. Chem. Phys., 11, 6465-6474, 10.5194/acp-11-6465-2011, 2011.

Nichman, L., Wolf, M., Davidovits, P., Onasch, T. B., Zhang, Y., Worsnop, D. R., Bhandari, J., Mazzoleni, C., and Cziczo, D. J.: Laboratory study of the heterogeneous ice nucleation on black-carbon-containing aerosol, Atmos. Chem. Phys., 19, 12175-12194, 10.5194/acp-19-12175-2019, 2019.

https://doi.org/10.5194/acp-2020-809
Preprint. Discussion started: 2 September 2020


Atmospheric Chemistry and Physics Discussions

Oh, C., and Sorensen, C. M.: The Effect of Overlap between Monomers on the Determination of Fractal Cluster Morphology, Journal of Colloid and Interface Science, 193, 17-25, https://doi.org/10.1006/jcis.1997.5046, 1997.

Onasch, T. B., Jayne, J. T., Herndon, S., Worsnop, D. R., Miake-Lye, R. C., Mortimer, I. P., and Anderson, B. E.: Chemical Properties of Aircraft Engine Particulate Exhaust Emissions, Journal of Propulsion and Power, 25, 1121-1137, 10.2514/1.36371, 2009.

Onasch, T. B., Trimborn, A., Fortner, E. C., Jayne, J. T., Kok, G. L., Williams, L. R., Davidovits, P., and Worsnop, D. R.: Soot Particle Aerosol Mass Spectrometer: Development, Validation, and Initial Application, Aerosol Science and Technology, 46, 804-817, 10.1080/02786826.2012.663948, 2012.

Pandis, S. N., Harley, R. A., Cass, G. R., and Seinfeld, J. H.: Secondary organic aerosol formation and transport, Atmospheric Environment. Part A. General Topics, 26, 2269-2282, https://doi.org/10.1016/0960-1686(92)90358-R, 1992.

Pereira, K. L., Rovelli, G., Song, Y. C., Mayhew, A. W., Reid, J. P., and Hamilton, J. F.: A new aerosol flow reactor to study secondary organic aerosol, Atmos. Meas. Tech., 12, 4519-4541, 10.5194/amt-12-4519-2019, 2019.

Persiantseva, N. M., Popovicheva, O. B., and Shonija, N. K.: Wetting and hydration of insoluble soot particles in the upper troposphere, Journal of Environmental Monitoring, 6, 939-945, 10.1039/B407770A, 2004.

Petzold, A., Ström, J., Ohlsson, S., and Schröder, F. P.: Elemental composition and morphology of ice-crystal residual particles in cirrus clouds and contrails, Atmospheric Research, 49, 21-34, https://doi.org/10.1016/S0169-8095(97)00083-5, 1998.

Pison, I., and Menut, L.: Quantification of the impact of aircraft traffic emissions on tropospheric ozone over Paris area, Atmospheric Environment, 38, 971-983, https://doi.org/10.1016/j.atmosenv.2003.10.056, 2004.

Popovicheva, O. B., Persiantseva, N. M., Lukhovitskaya, E. E., Shonija, N. K., Zubareva, N. A., Demirdjian, B., Ferry, D., and Suzanne, J.: Aircraft engine soot as contrail nuclei, Geophysical Research Letters, 31, doi:10.1029/2003GL018888, 2004.

Presto, A. A., Miracolo, M. A., Donahue, N. M., and Robinson, A. L.: Secondary Organic Aerosol Formation from High-NOx Photo-Oxidation of Low Volatility Precursors: n-Alkanes, Environmental science & technology, 44, 2029-2034, 10.1021/es903712r, 2010.

Pruppacher, H. R., and Klett, J. D.: Microphysics of Clouds and Precipitation, 2 ed., Atmospheric and Oceanographic Sciences Library, 18, Springer Netherlands, XXII, 954 pp., 2010.

Ramachandran, G., and Reist, P. C.: Characterization of Morphological Changes in Agglomerates Subject to Condensation and Evaporation Using Multiple Fractal Dimensions, Aerosol Science and Technology, 23, 431-442, 10.1080/02786829508965326, 1995.

Samson, R. J., Mulholland, G. W., and Gentry, J. W.: Structural analysis of soot agglomerates, Langmuir, 3, 272-281, 10.1021/la00074a022, 1987.

Schilling, K. A., Yee, L. D., Loza, C. L., Coggon, M. M., Schwantes, R., Zhang, X., Dalleska, N. F., and Seinfeld, J. H.: Secondary Organic Aerosol Composition from C12 Alkanes, The Journal of Physical Chemistry A, 119, 4281-4297, 10.1021/jp501779w, 2015.

https://doi.org/10.5194/acp-2020-809
Preprint. Discussion started: 2 September 2020


Atmospheric Chemistry and Physics Discussions

Seinfeld, J. H.: Clouds, contrails and climate, Nature, 391, 837-838, 1998.

Shu, Y., and Atkinson, R.: Rate constants for the gas-phase reactions of O3 with a series of Terpenes and OH radical formation from the O3 reactions with Sesquiterpenes at 296 ± 2 K, International Journal of Chemical Kinetics, 26, 1193-1205, 10.1002/kin.550261207, 1994.

Simonen, P., Saukko, E., Karjalainen, P., Timonen, H., Bloss, M., Aakko-Saksa, P., Rönkkö, T., Keskinen, J., and Dal Maso, M.: A new oxidation flow reactor for measuring secondary aerosol formation of rapidly changing emission sources, Atmos. Meas. Tech., 10, 1519-1537, 10.5194/amt-10-1519-2017, 2017.

Slowik, J. G., Cross, E. S., Han, J.-H., Kolucki, J., Davidovits, P., Williams, L. R., Onasch, T. B., Jayne, J. T., Kolb, C. E., and Worsnop, D. R.: Measurements of Morphology Changes of Fractal Soot Particles using Coating and Denuding Experiments: Implications for Optical Absorption and Atmospheric Lifetime, Aerosol Science and Technology, 41, 734-750, 10.1080/02786820701432632, 2007.

Timko, M. T., Albo, S. E., Onasch, T. B., Fortner, E. C., Yu, Z., Miake-Lye, R. C., Canagaratna, M. R., Ng, N. L., and Worsnop, D. R.: Composition and Sources of the Organic Particle Emissions from Aircraft Engines, Aerosol Science and Technology, 48, 61-73, 10.1080/02786826.2013.857758, 2014.

Tritscher, T., Jurányi, Z., Martin, M., Chirico, R., Gysel, M., Heringa, M. F., DeCarlo, P. F., Sierau, B., Prévôt, A. S. H., Weingartner, E., and Baltensperger, U.: Changes of hygroscopicity and morphology during ageing of diesel soot, Environmental Research Letters, 6, 034026, 10.1088/1748-9326/6/3/034026, 2011.

Tully, F. P., Ravishankara, A. R., Thompson, R. L., Nicovich, J. M., Shah, R. C., Kreutter, N. M., and Wine, P. H.: Kinetics of the reactions of hydroxyl radical with benzene and toluene, The Journal of Physical Chemistry, 85, 2262-2269, 10.1021/j150615a025, 1981.

Vali, G., DeMott, P. J., Möhler, O., and Whale, T. F.: Technical Note: A proposal for ice nucleation terminology, Atmos. Chem. Phys., 15, 10263-10270, 10.5194/acp-15-10263-2015, 2015.

Vander Wal, R. L., Bryg, V. M., and Huang, C.-H.: Aircraft engine particulate matter: Macro- micro- and nanostructure by HRTEM and chemistry by XPS, Combustion and Flame, 161, 602-611, 10.1016/j.combustflame.2013.09.003, 2014.

Wang, B., Lambe, A. T., Massoli, P., Onasch, T. B., Davidovits, P., Worsnop, D. R., and Knopf, D. A.: The deposition ice nucleation and immersion freezing potential of amorphous secondary organic aerosol: Pathways for ice and mixed-phase cloud formation, Journal of Geophysical Research: Atmospheres, 117, n/a-n/a, 10.1029/2012jd018063, 2012.

Wang, Y., Liu, F., He, C., Bi, L., Cheng, T., Wang, Z., Zhang, H., Zhang, X., Shi, Z., and Li, W.: Fractal Dimensions and Mixing Structures of Soot Particles during Atmospheric Processing, Environmental Science & Technology Letters, 4, 487-493, 10.1021/acs.estlett.7b00418, 2017.

Wolf, M. J., Coe, A., Dove, L. A., Zawadowicz, M. A., Dooley, K., Biller, S. J., Zhang, Y., Chisholm, S. W., and Cziczo, D. J.: Investigating the Heterogeneous Ice Nucleation of Sea Spray Aerosols Using Prochlorococcus as a Model Source of Marine Organic Matter, Environmental science & technology, 53, 1139-1149, 10.1021/acs.est.8b05150, 2019.

https://doi.org/10.5194/acp-2020-809
Preprint. Discussion started: 2 September 2020

Yee, L. D., Craven, J. S., Loza, C. L., Schilling, K. A., Ng, N. L., Canagaratna, M. R., Ziemann, P. J., Flagan, R. C., and Seinfeld, J. H.: Effect of chemical structure on secondary organic aerosol formation from C₁₂ alkanes, Atmos. Chem. Phys., 13, 11121-11140, 10.5194/acp-13-11121-2013, 2013.

Zawadowicz, M. A., Abdelmonem, A., Mohr, C., Saathoff, H., Froyd, K. D., Murphy, D. M., Leisner, T., and Cziczo, D. J.: Single-Particle Time-of-Flight Mass Spectrometry Utilizing a Femtosecond Desorption and Ionization Laser, Analytical Chemistry, 87, 12221-12229, 10.1021/acs.analchem.5b03158, 2015.

Zhang, C., Hui, X., Lin, Y., and Sung, C.-J.: Recent development in studies of alternative jet fuel combustion: Progress, challenges, and opportunities, Renewable and Sustainable Energy Reviews, 54, 120-138, 10.1016/j.rser.2015.09.056, 2016.

Zhang, X., Chen, X., and Wang, J.: A number-based inventory of size-resolved black carbon particle emissions by global civil aviation, Nature communications, 10, 534, 10.1038/s41467-019-08491-9, 2019a.

Zhang, Y., Chen, Y., Lambe, A. T., Olson, N. E., Lei, Z., Craig, R. L., Zhang, Z., Gold, A., Onasch, T. B., Jayne, J. T., Worsnop, D. R., Gaston, C. J., Thornton, J. A., Vizuete, W., Ault, A. P., and Surratt, J. D.: Effect of the Aerosol-Phase State on Secondary Organic Aerosol Formation from the Reactive Uptake of Isoprene-Derived Epoxydiols (IEPOX), Environmental Science & Technology Letters, 5, 167-174, 10.1021/acs.estlett.8b00044, 2018a.

Zhang, Y., Katira, S., Lee, A., Lambe, A. T., Onasch, T. B., Xu, W., Brooks, W. A., Canagaratna, M. R., Freedman, A., Jayne, J. T., Worsnop, D. R., Davidovits, P., Chandler, D., and Kolb, C. E.: Kinetically controlled glass transition measurement of organic aerosol thin films using broadband dielectric spectroscopy, Atmos. Meas. Tech., 11, 3479-3490, 10.5194/amt-11-3479-2018, 2018b.

Zhang, Y., Liu, F., Clavel, D., Smallwood, G. J., and Lou, C.: Measurement of soot volume fraction and primary particle diameter in oxygen enriched ethylene diffusion flames using the laser-induced incandescence technique, Energy, 177, 421-432, https://doi.org/10.1016/j.energy.2019.04.062, 2019b.

Zhang, Y., Nichman, L., Spencer, P., Jung, J. I., Lee, A., Heffernan, B. K., Gold, A., Zhang, Z., Chen, Y., Canagaratna, M. R., Jayne, J. T., Worsnop, D. R., Onasch, T. B., Surratt, J. D., Chandler, D., Davidovits, P., and Kolb, C. E.: The Cooling Rate- and Volatility-Dependent Glass-Forming Properties of Organic Aerosols Measured by Broadband Dielectric Spectroscopy, Environmental science & technology, 53, 12366-12378, 10.1021/acs.est.9b03317, 2019c.

Zhao, D. F., Buchholz, A., Kortner, B., Schlag, P., Rubach, F., Fuchs, H., Kiendler-Scharr, A., Tillmann, R., Wahner, A., Watne, Å. K., Hallquist, M., Flores, J. M., Rudich, Y., Kristensen, K., Hansen, A. M. K., Glasius, M., Kourtchev, I., Kalberer, M., and Mentel, T. F.: Cloud condensation nuclei activity, droplet growth kinetics, and hygroscopicity of biogenic and anthropogenic secondary organic aerosol (SOA), Atmos. Chem. Phys., 16, 1105-1121, 10.5194/acp-16-1105-2016, 2016.

Zhao, L., Yang, T., Kaiser, R. I., Troy, T. P., Ahmed, M., Ribeiro, J. M., Belisario-Lara, D., and Mebel, A. M.: Combined Experimental and Computational Study on the Unimolecular Decomposition of JP-8 Jet Fuel Surrogates. II: n-Dodecane (n-C12H26), The Journal of Physical Chemistry A, 121, 1281-1297, 10.1021/acs.jpca.6b11817, 2017.